Max-Planck-Institut für Meteorologie

REPORT No. 179

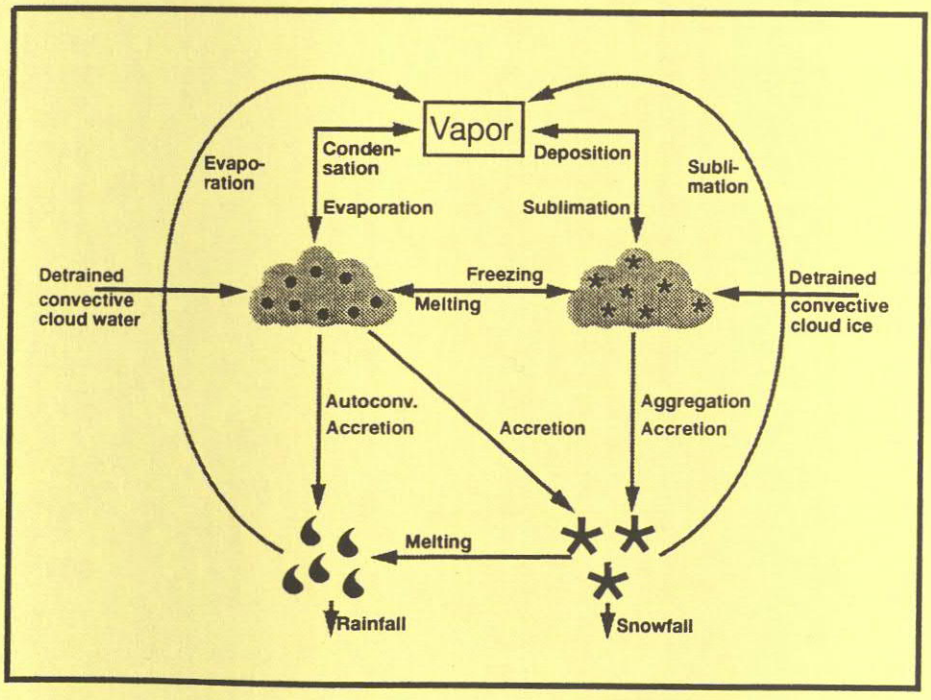

INTRODUCTION OF A PROGNOSTIC CLOUD ICE SCHEME IN THE ECHAM GENERAL CIRCULATION MODEL: IMPACT ON CLIMATE AND CLIMATE SENSITIVITY

by

ULRIKE LOHMANN · ERICH ROECKNER

HAMBURG, November 1995

AUTHORS:

Ulrike Lohmann
Erich Roeckner

Max-Planck-Institut
für Meteorologie

MAX-PLANCK-INSTITUT
FÜR METEOROLOGIE
BUNDESSTRASSE 55
D-20146 Hamburg
F.R. GERMANY

Tel.: +49-(0)40-4 11 73-0
Telefax: +49-(0)40-4 11 73-298
E-Mail: <name> @ dkrz.d400.de

REPh 179

ISSN 0937-1060

Introduction of a prognostic cloud ice scheme in the ECHAM general circulation model: Impact on climate and climate sensitivity

Ulrike Lohmann and Erich Roeckner
Max Planck Institute for Meteorology, Hamburg, Germany

Abstract. A new cloud microphysics scheme including a prognostic treatment of cloud ice (PCI) is developed to yield a more physically based representation of the components of the atmospheric moisture budget in the general circulation model ECHAM. The new approach considers cloud water and cloud ice as separate prognostic variables. A precipitation formation which can distinguish between maritime and continental clouds by considering the cloud droplet number concentration in addition to the cloud water content is introduced. Based on different observational data sets, the cloud droplet number concentration is proportional to the sulfate aerosol mass concentration as given from the simulated sulfur cycle with ECHAM.

Results obtained from the new scheme are compared to satellite observations and in-situ measurements of cloud physical and radiative properties. In general the standard model ECHAM4 and also PCI capture the overall features and the simulated distributions usually lie within the range of observed uncertainty, which is unfortunately very high. As compared to ECHAM4, only slight improvements are achieved with the new scheme, e.g. the overestimated cloud liquid water path over convectively active regions is eliminated in PCI. On the other hand, some shortcomings, e.g. too high shortwave cloud forcings over subtropical subsidence regions occur.

Cloud radiation feedbacks are known to induce large uncertainties on climate sensitivity in climate change experiments. Therefore emphasis is laid on the influence of the prognostic cloud scheme versus the standard scheme on the global climate sensitivity. In the climate change experiment with ECHAM4 the global climate sensitivity is 20% higher than in the clear-sky reference atmosphere because the increase of total water path and of cirrus emissivity in the warmer atmosphere contributes substantially to the overall positive cloud feedback. In PCI the ice water path slightly decreases. Thus the cloud feedback is zero, i.e. the global climate sensitivity is the same as in the clear-sky reference atmosphere.

1. Introduction

About 50% of the Earth's surface is covered with clouds. They are the most important regulator of the Earth's radiation budget, that is, clouds cool the earth-atmosphere by 48 Wm^{-2} in the visible wavelengths and warm it by 30 Wm^{-2} in the infrared as derived from measurements of the Earth Radiation Budget Experiment (ERBE) (Collins et al., 1994). Additionally, clouds exert a major impact on the hydrological cycle and they affect the dynamics of the atmosphere through complex couplings among radiative, thermodynamic, and dynamic processes (Arakawa, 1975). However, the lack of understanding of clouds remains one of the largest uncertainties in climate modeling and prediction (Gates, 1992; IPCC, 1992). The different considerations of cloud processes in general circulation models (GCM) is still one of the main reasons for differences in climate sensitivity (Cess et al., 1990). Cloud properties span more than ten orders of magnitude, where most of these processes are below the resolved scales of GCMs.

Various parameterizations have been developed to represent clouds and their radiative effects in GCMs. The earliest approach uses a fixed geographical distribution of cloud fraction and cloud optical depth (e.g. Manabe et al., 1965; Boer et al., 1984). A more advanced method is to diagnose cloud cover from large-scale variables such as relative humidity (Geleyn, 1981) or additionally from vertical velocity, precipitation rate and strength of inversion (Slingo, 1987). This approach has frequently been used in many GCMs, e.g. Slingo (1987); McFarlane et al. (1992); Kiehl et al. (1994). The most recent trend is to obtain cloud water/ice from the respective transport equation following the pioneering work of Sundqvist (1978). In conjunction with that, cloud microphysical processes are parameterized in different stages of complexity. This approach is in principle the most physically realistic. However, the introduction of complex cloud microphysical processes which cannot be resolved on spatial and temporal scales of a GCM introduces more degrees of freedom. A prognostic scheme for cloud water and cloud ice together has been introduced, for instance, by Roeckner and Schlese (1985); LeTreut and Li (1988); Smith (1990); Del Genio et al. (1995). Cloud water and cloud ice are treated separately by Lee et al. (1992) and Ose (1993). The most complex approach implemented in a GCM so far is given in Fowler et al. (1995), who prognose cloud water, cloud ice, rain and snow. Further details about the different approaches and their realization in different GCMs can be found in Fowler et al. (1995).

In the current version of the Hamburg GCM (ECHAM4) only one prognostic equation for

cloud water and cloud ice together is considered following Sundqvist (1978). Mixed cloud phase is always assumed between -40°C and 0°C and the ratio of cloud water to cloud ice depends on temperature (Rockel et al., 1991). However, observational data show that the probability of occurrence of supercooled water clouds or pure ice clouds between -40°C and 0°C is not negligible (Matveev, 1984). Rangno and Hobbs (1994) show that cloud droplet size is a more reliable predictor than temperature of whether a cloud would glaciate. To allow for interactions between cloud droplets and ice crystals, the new approach considers cloud ice as a separate prognostic variable in addition to water vapor and cloud liquid water similar to Lee et al. (1992), Ose (1993) and Fowler et al. (1995).

The three studies cited above use parameterizations of the autoconversion rate of cloud droplets to rain drops which depend only on the mass mixing ratio of cloud water based on Kessler (1969) or Sundqvist (1978). However, cloud droplet spectra in maritime and continental clouds are very different. Aerosol particles such as sulfate aerosols can act as cloud condensation nuclei (CCN). The CCN spectrum and the water vapor supply in a cloud determine the cloud droplet number concentration (N_l). The characteristic of a typical continental cloud is a narrow droplet spectrum with many small droplets resulting from high levels of CCN. Maritime clouds typically have a broader spectrum with fewer and larger droplets, because fewer CCN are available (Pruppacher and Klett, 1978). The precipitation formation in the warm phase depends mainly on the concentration of large droplets which is usually anticorrelated to N_l (e.g. Albrecht, 1989; Fouquart and Isaka, 1992). Shiptrack observations reported by Radke et al. (1989); King et al. (1993), for example, reveal a simultaneous increase in N_l and cloud water content of clouds compared to adjacent clouds. Thus the growth of large droplets by collision in clouds in the track is suppressed, and in turn the development of drizzle is prevented. Parameterizations which account for the dependence of the precipitation formation on N_l are developed by e.g. Berry and Reinhardt (1973); Chen and Cotton (1987) and Beheng (1994). Boucher et al. (1995) have implemented a similar approach as Chen and Cotton (1987) in their GCM and have investigated the amount of water stored in the atmosphere and the cloud radiative properties in relation to different prescribed values of N_l. We have introduced Beheng's (1994) parameterization of the autoconversion rate, which is derived from the stochastic collection equation. Instead of prescribing N_l, we relate N_l based on different observational data sets to the sulfate aerosol mass (Boucher and Lohmann, 1995). A similar approach is taken for the conversion rate from cloud ice to snow by aggregation (Levkov et al., 1992). Unlike the parameterizations commonly used for the aggregation of ice crystals to snow (e.g. Kessler,

1969; Rutledge and Hobbs, 1983), Levkov et al. (1992) avoid a threshold formulation and consider additionally the dependence on ice crystal size.

Mitchell et al. (1989) have performed some $2*CO_2$ simulations with different cloud schemes in the GCM of the United Kingdom Meteorological Office (UKMO). Their model is very sensitive to changes in cloud parameters. With a diagnostic cloud approach (i.e. cloud cover is a function of relative humidity) and constant cloud optical depth, the surface temperature increases by ΔT_s=5.2K. Including an explicit cloud water variable and remaining the optical depth constant, reduces the increase in warming to ΔT_s=2.7K. With cloud radiative properties depending on the cloud water content the warming is further reduced to ΔT_s=1.9K. Lohmann and Roeckner (1995) show that cirrus cloud radiative properties have a significant influence on the global climate sensitivity realized by an increase in sea surface temperature by uniformly 4K, in the spirit of the investigation by Cess et al. (1990). If cirrus clouds are assumed to be transparent the cloud feedback is negative, while it is positive with computed cirrus emissivity as well as if cirrus clouds are assumed to be black (Lohmann and Roeckner, 1995). In this study we investigate the impact on global climate sensitivity of a physically more advanced cloud scheme.

The cloud microphysics scheme developed to yield a more physically based representation of the components of the atmospheric moisture budget in the ECHAM model is described in section 2. In addition, the changes in the cloud radiative properties are discussed. The effects of the cloud microphysics scheme on some hydrologic variables and on the radiation budget are analyzed in section 3. In section 4 the influence of the different cloud schemes on climate sensitivity is presented. A summary of the basic results and conclusions are given in section 5.

2. Model description

The dynamics and part of the model physics of the ECHAM model have been adopted from the European Centre for Medium-Range Weather Forecasts (ECMWF) model (Roeckner et al., 1992). Prognostic variables are vorticity, divergence, temperature, (logarithm of) surface pressure, and the mass mixing ratios of water vapor, and additionally large-scale cloud water and cloud ice. The model equations are solved on 19 vertical levels in a hybrid p-σ-system by using the spectral transform method with triangular truncation at wavenumber 30 (T30). Nonlinear terms and physical processes are evaluated at grid points of a "Gaussian grid" providing a nominal resolution of 3.75° x 3.75°. A semi-implicit leap frog time integration scheme with Δt=30 minutes is used for the simulation with T30 resolution. Different from previous versions, ECHAM4 uses a semi-Lagrangian technique (Rasch and Williamson, 1990) for computing the horizontal and vertical advection of positive definite quantities such as water vapor and cloud water. However, in the new scheme, which includes a prognostic treatment of cloud ice (PCI) the advection of cloud water and cloud ice is omitted for convenience, because sensitivity experiments have shown that their contribution is at most 10% of the microphysical sources and sinks. Cumulus clouds are represented by a bulk model including the effects of entrainment and detrainment on the updraft and downdraft convective mass fluxes (Tiedtke, 1989). An adjustment closure based on the convective available potential energy (CAPE) is used (Nordeng, 1995). Organized entrainment is assumed to depend on buoyancy, and the parameterization of organized detrainment is based upon a cloud population hypothesis. The turbulent transfer of momentum, heat, water vapor, and cloud water is calculated on the basis of a higher-order closure scheme (Brinkop and Roeckner, 1995). A new global set of land-surface parameters, including surface background albedo, surface roughness length, leaf area index, fractional vegetation cover, and forest ratio (Claussen et al., 1994) is used.

2.1. Cloud Microphysics

The bulk microphysics parameterizations in the new scheme bases mainly on Beheng (1994) for warm phase processes, while the parameterizations of the mixed and ice phase follows Levkov et al. (1992), developed for a mesoscale model. The parameterizations are necessarily scale-dependent and some simplifications are required. The terminal velocity of cloud water and cloud ice is neglected as introduced in the pioneering work of Kessler (1969). Following Ghan and Easter (1992) and Mölders et al. (1994), rain and snow are treated diagnostically. They find that by diagnosing rather than predicting rain and snow, the permissible time step is

increased tenfold with little loss in accuracy. Differences in form and structure of ice and snow crystals are neglected: "pristine" non-aggregated ice particles and single snow crystals are assumed. The shapes of all hydrometeors are considered to be spherical. Sundqvist (1978) has developed a formalism to include fractional cloud cover in a prognostic scheme. Its framework has been used in all ECHAM versions (Roeckner et al. 1992) and has been adopted by the new scheme as well. The governing equations for water vapor (q_v), cloud water (q_l) and cloud ice (q_i), respectively, are:

$$\partial q_v/\partial t = R(q_v) + b\left(Q^c_{cnd} + Q^c_{dep}\right) + (1-b)\left(Q^o_{evp} - Q^o_{cnd} - Q^o_{dep}\right) \quad (1)$$

$$\partial q_l/\partial t = R(q_l) + b\left(Q^c_{cnd} - Q^c_{aut} - Q^c_{racl} - Q^c_{sacl} - Q^c_{frz} + Q^c_{mlt}\right) + (1-b)\,Q^o_{cnd} \quad (2)$$

$$\partial q_i/\partial t = R(q_i) + b\left(Q^c_{dep} - Q^c_{agg} - Q^c_{saci} + Q^c_{frz} - Q^c_{mlt}\right) + (1-b)\,Q^o_{dep} \quad (3)$$

where R(...) denotes the sum over all transport terms of q_v, q_l, and q_i respectively, including advection of water vapor, turbulence and convection (detrainment at the top of cumulus clouds) and b is the fractional cloud cover. The superscripts (c) and (o) refer to the cloudy and cloud-free part of the grid box, respectively. The cloud-microphysical processes simulated in the new scheme are condensation of water vapor and evaporation of cloud water in the cloudy part (Q^c_{cnd}), deposition of water vapor and sublimation of cloud ice in the cloudy part (Q^c_{dep}), evaporation of cloud water (Q^o_{cnd}) and sublimation of cloud ice (Q^o_{dep}) transported into the cloud-free part of a grid box, evaporation and sublimation of precipitation (Q^o_{evp}), autoconversion of cloud droplets (Q^c_{aut}), accretion of cloud droplets by rain (Q^c_{racl}), of cloud droplets by snow (Q^c_{sacl}), of ice crystals by snow (Q^c_{saci}), homogeneous, heterogeneous, and contact freezing of cloud droplets (Q^c_{frz}), aggregation of ice crystals (Q^c_{agg}), and melting of cloud ice (Q^c_{mlt}). For simplicity the superscripts have been left out in the following.

Fractional cloud cover b is obtained by an empirical function of relative humidity (Sundqvist et al., 1989):

$$b = 1 - \sqrt{1 - b_o} \text{ with } b_o = (r - r_o)/(1 - r_o) \quad (4)$$

where r is the grid-mean relative humidity and r_o is a condensation threshold which is specified as a function of height following Xu and Krueger (1991). Condensational growth of cloud droplets or depositional growth of ice crystals occur if $r > r_o$. Conversely, an existing cloud is diluted by evaporation or sublimation, if $r < r_o$. The moisture transported into a grid box with

fractional cloud cover b is used partly for condensation or deposition and partly for moistening of the cloud-free area with b being the weighting factor (Sundqvist, 1978). It is assumed that there are always sufficient condensation nuclei or ice nuclei to initiate condensation and deposition. Depositional growth of water vapor on ice crystals (Q_{dep}) always takes place at temperatures below -35°C. Above -35° Q_{dep} only is a source for cloud ice, in case cloud ice is already present. Then saturation with respect to ice is assumed. Apart from that, water vapor condenses on cloud droplets at temperatures above -35°. Subsequently, cloud droplets can be transformed into ice crystals by heterogeneous or contact freezing. Thus saturation with respect to water is assumed.

The precipitation formation (autoconversion of cloud droplets) distinguishes between maritime and continental clouds by considering the cloud droplet number concentration (N_l) in addition to the cloud water content (Beheng, 1994). It is derived from the stochastic collection equation, which describes the time evolution of a droplet spectrum changing by collisions among droplets of different size. The autoconversion rate in SI-units is given by:

$$Q_{aut} = \left(\gamma_1 \cdot 6 \cdot 10^{28} n^{-1.7} \left(10^{-6} N_l\right)^{-3.3} \left(10^{-3} \rho q_{cl}\right)^{4.7}\right) / \rho \qquad (5)$$

where n (=10) is the width of the initial cloud droplet spectrum, described by a Gamma function, ρ is the air density and q_{cl} is the in-cloud water content ($q_{cl}=q_l/b$). γ_1 (=10) is a microphysical constant which determines the efficiency of rain formation and, thus, the cloud lifetime. At present N_l cannot be computed realistically in GCMs because it depends on several factors which are not easy to predict, such as subgrid-scale velocity, maximum supersaturation, and availability of CCN. Therefore we empirically relate N_l to the sulfate aerosol mass (mSO_4^{2-}) (Boucher and Lohmann, 1995). The monthly mean values of mSO_4^{2-} are given from a sulfur cycle simulation with ECHAM (Feichter et al.,1995). Measurements of mSO_4^{2-}, CCN and N_l are taken at various continental and marine sites in clean and polluted air, for a variety of weather situations. Hence, empirical relationships between N_l and mSO_4^{2-} are derived for maritime and continental clouds:

$$N_l^{mar} = 10^6 \cdot 10^{2.06 + 0.48 \log (mSO_4^{2-})} \qquad (6)$$

$$N_l^{cont} = 10^6 \cdot 10^{2.24 + 0.257 \log (mSO_4^{2-})} \qquad (7)$$

Figure 1 shows the geographical distribution of N_l in model level 15 (approximately 850 hPa) for January and July. Maxima in N_l are associated with high sulfur emissions due to industrial

activity, e.g. North America, Europe and southeast Asia. The concentration over remote oceanic regions ranges between 30 and 90 droplets cm^{-3}. High levels of mSO_4^{2-} are transported downwind the industrial centers off the shores of the Asian and North American coast, yielding high concentrations of N_l. In July mSO_4^{2-} and, hence, N_l over the northern hemisphere is higher, because more oxidants are available to form SO_4^{2-} and less SO_4^{2-} is washed and rained out (Feichter et al., 1995).

Raindrops, once formed, continue to grow by accretion of cloud water. The accretion rate is derived from the stochastic collection equation (Beheng, 1994):

$$Q_{racl} = a_1 \cdot \rho \cdot q_{cl} \cdot q_r \tag{8}$$

with q_r is the rain content and $a_1 = 6\ s^{-1}$.

At temperatures below -35°C the total amount of cloud water freezes homogeneously and instantaneously to cloud ice (Lord et al. 1984; Eppel et al., 1995):

$$Q_{frz} = q_{cl}/\Delta t \tag{9}$$

For heterogeneous freezing of cloud droplets between 0°C and -35°C we use the extrapolated Bigg's (1953) equation down to the cloud droplet size (Levkov et al., 1992; Murakami, 1990):

$$Q_{frz} = a_2 \{ \exp [b_2 (T_o - T)] - 1 \} \frac{\rho q_{cl}^2}{\rho_l N_l} \tag{10}$$

where a_2 (=100 $m^{-3}s^{-1}$) and b_2 (=0.66 K^{-1}) are determined from laboratory experiments. ρ_l (=1000 kg m^{-3}) is the density of water, T the grid-mean temperature and T_o=273.16 K.

Brownian-diffusion contact nucleation results from the random collision of aerosol particles with supercooled cloud droplets. It may be written as (Levkov et al., 1992; Cotton et al.,1986):

$$Q_{frz} = m_{io} F_1 DF_{ar} \tag{11}$$

with DF_{ar} (=4*10^{-7} m^2s^{-1}) is the aerosol diffusivity, m_{io} (=1*10^{-12} kg) is the initial mass of a nucleated ice crystal, and

$$F_1 = 4\pi r_{l,v} N_l N_a / \rho \tag{12}$$

The concentration of active contact nuclei is approximated to $N_a=N_{ao}(270.15-T)$, with N_{ao}= 2*10^5 m^{-3} and $r_{l,v}$ is the mean volume cloud droplet radius:

$$r_{l,v} = \sqrt[3]{\frac{3q_{cl}\rho}{4\pi\rho_l N_l}} \tag{13}$$

The conversion rate from cloud ice to snow by aggregation of ice crystals according to Levkov et al., (1992) based on work of Murakami (1990) is given by:

$$Q_{agg} = \gamma_2 q_{ci}/\Delta t_1 \tag{14}$$

where q_{ci} is the in-cloud ice content, γ_2 (=180) is again a microphysical constant which determines the efficiency of snow formation and, thus, the ice cloud lifetime and Δt_1 is equal to the time needed for the cloud ice concentration to decrease from N_i to $N_i(r_{i,v}/r_{so})^3$:

$$\Delta t_1 = -\frac{2}{c_1}\log\left(\frac{r_{i,v}}{r_{so}}\right)^3 \tag{15}$$

r_{so} (=10^{-4} m) is the smallest radius of a particle in the snow class and

$$c_1 = \frac{q_{ci}\rho a_3 E_{ii} X}{\rho_i}\left(\frac{\rho_o}{\rho}\right)^{0.33} \tag{16}$$

with X (=0.25) is the dispersion of the fall velocity spectrum of cloud ice, E_{ii} (=0.1) is the collection efficiency between ice crystals, ρ_o (=1.3 kg m^{-3}) is the air density at the surface, a_3 (=700 s^{-1}) is an empirical constant (Murakami, 1990), and $r_{i,v}$ is the mean volume radius. Moss et al. (1995) derived an empirical relationship between the effective radius ($r_{i,e}$) of an ice crystal distribution and the ice content based on aircraft observations of frontal clouds around the British Isles:

$$r_{i,e} = 8.38*10^{-5}\left(10^3 \rho q_{ci}\right)^{0.216} \tag{17}$$

Moss et al. (1995) measured simultaneously $r_{i,e}$ and $r_{i,v}$ yielding a quadratic relationship between the two:

$$r_{i,e}^3 = a_4\left(10^{-6} r_{i,v}\right)^3 + b_4\left(10^{-6} r_{i,v}\right)^6 \tag{18}$$

where a_4=1.61 and b_4=3.56*10^{-4}.

The parameterization of the accretional growth of snow (riming and collecting ice crystals) according to Levkov et al. (1992) is based on Lin et al. (1983). Snow crystals are assumed to be distributed exponentially (Gunn and Marshall, 1958):

$$n_s(D_s) = n_{os} \exp(-\lambda_s D_s) \tag{19}$$

where $n_s(D_s)$ is the concentration of particles of diameter D_s per unit size interval. D_s is the diameter of the water drop formed by the melting snow particle. n_{os} (=3*10^6 m^{-4}) is the intercept parameter obtained from measurements (Gunn and Marshall, 1958). λ_s is the slope of the particle size distribution and is written as (Potter, 1991):

$$\lambda_s = \left(\frac{\pi \rho_l n_{os}}{\rho q_s} \right)^{0.25} \tag{20}$$

where q_s is the snow content. Snow crystals settle through a population of supercooled cloud droplets, colliding and coalescing with them (riming). The rate of change in the mixing ratio for snow is based on the geometric sweep-out concept integrated over all snow sizes for the assumed snow size distribution given in Eq. (19):

$$Q_{sacl} = \gamma_3 \frac{\pi E_{sl} n_{os} a_5 q_{cl} \Gamma(3 + b_5)}{4 \lambda_s^{3 + b_5}} \left(\frac{\rho_o}{\rho} \right)^{0.5} \tag{21}$$

where a_5=4.83, b_5=0.25 and E_{sl} (=1) is the collection efficiency of snow for cloud droplets (Lin et al., 1983). Levkov et al. (1992) limited the riming process to cloud water contents above 10^{-5} kg kg^{-1}. Instead of this, we have chosen γ_3 (=0.1).

The accretion rate of ice crystals by snow is similar to Eq. (21) and is expressed as:

$$Q_{saci} = \frac{\pi E_{si} n_{os} a_5 q_{ci} \Gamma(3 + b_5)}{4 \lambda_s^{3 + b_5}} \left(\frac{\rho_o}{\rho} \right)^{0.5} \tag{22}$$

The collection efficiency of snow for cloud ice (E_{si}) is assumed to be temperature dependent:

$$E_{si} = \exp(0.25 (T - T_o)) \tag{23}$$

All ice crystals melt immediately when the temperature is above 0°C (Fowler et al., 1995):

$$Q_{mlt} = q_{ci} / \Delta t \tag{24}$$

The total sum of precipitation is then given by the sum of Eqs. (5), (8), (14), (21) and (22). Precipitation falling into the cloud-free part of a grid box is exposed to evaporation or sublimation, which is parameterized in term of the saturation deficit (Roeckner et al., 1992):

$$Q_{evp} = -\frac{1}{\Delta t}\frac{\gamma_4 (q_v - q_{vs})}{1 + \frac{L}{c_p}\frac{dq_{vs}}{dT}} \qquad (25)$$

where γ_4 (=0.15) is a tunable parameter, q_{vs} is the saturation water vapor, L (=2.5008*10^6 J kg^{-1} or 2.8345*10^6 J kg^{-1}) the latent heat of vaporization or sublimation, respectively, and c_p is the specific heat of moist air at constant pressure.

Melting of snow occurs when the temperature exceeds 2°C based on observational data by Mason (1971). It is not only limited by the snow amount, but also by keeping the cooling of the layer linked to this, such that the temperature of the layer after melting is not lower than 2°C (Roeckner et al., 1992).

2.2. Cloud Radiative Properties

The radiation code of ECHAM4 is based on a two-stream solution of the radiative transfer equation with six spectral intervals in the terrestrial infrared spectrum (Morcrette, 1991) and two in the solar part of the spectrum (Fouquart and Bonnel, 1980). Gaseous absorption due to water vapor, CO_2, O_3, CH_4, N_2O, and CFCs is included, as well as scattering and absorption due to prescribed aerosols and model-generated clouds. The single scattering properties of water droplets and ice crystals are derived from Mie theory, and the results are fitted to the spectral resolution of the radiation model and formulated in terms of cloud droplet and ice crystal effective radii (Rockel et al., 1991). For liquid clouds, the mean volume cloud droplet radius (r_c) is calculated according to Eq. (13) from the in-cloud liquid water content (q_{cl}) and the cloud droplet number concentration (N_l) as defined in Eqs. (6) and (7). Note that different from PCI an idealized distribution of N_l is used in ECHAM4 with different values for continental clouds (N_l=220 cm^{-3}) and maritime clouds (N_l=100 cm^{-3}) in the planetary boundary layer. Above the boundary layer, a gradual reduction to N_l=50 cm^{-3} in upper layers is assumed. Simultaneous measurements of $r_{l,c}$ and the effective radius of cloud droplets ($r_{l,e}$) suggest a linear regression between the two radii:

$$r_{l,e} = k\, r_{l,v} \qquad (26)$$

with k=1.143 for continental clouds and k=1.077 for maritime clouds (Johnson, 1993).

The effective radius of ice crystals is defined according to Eq. (17).

3. Results

The results presented below are based on a five-year integration with the standard cloud scheme in ECHAM4 and with the prognostic cloud ice scheme (PCI) at T30 resolution with prescribed observed sea surface temperatures and sea ice extents for the period 1985-1989 from the atmospheric model intercomparison project (AMIP) data set (Gates, 1992) after a three month spin-up time. A climatological comparison of the simulations of clouds and the radiation budget including short-term and long-term variability from ECHAM4 with observations is given in Chen and Roeckner (1995). We only focus on mean quantities.

3.1. Global means

			Obs		ECHAM4		PCI	
			Jan	Jul	Jan	Jul	Jan	Jul
WVM	[kg m^{-2}]	SSM/I (Ewald&Schlüssel, 1995)	29	29	29	30	31	32
LWP	[g m^{-2}]	SSM/I (Greenwald et al., 1993)	78	84	78	80	79	77
		SSM/I (Weng&Grody, 1995)	51	53				
IWP	[g m^{-2}]				18	21	28	30
TCC	[%]	ISCCP	62	60	64	60	64	60
		Surface observations (Hahn et al., 1994)	62	62				
SCF	[W m^{-2}]	ERBE	-52	-48	-55	-49	-50	-44
LCF	[W m^{-2}]	ERBE	29	29	27	29	30	30

Table 1: Globally-averaged values of water vapor mass (WVM), liquid water path (LWP), ice water path (IWP), total cloud cover (TCC), shortwave (SCF) and longwave (LCF) cloud forcing from model simulations (ECHAM4 and PCI) and observations, for January and July. Note that global values of WVM, LWP and IWP are restricted to oceans between 60°S and 60°N. Uncertainties of the observations are estimated to be 5 Wm^{-2} for ERBE, 4.4 kg m^{-2} for individual measurements of WVM, 5% regional bias (higher in polar regions) for ISCCP, and the two estimations of LWP suggest an uncertainty of about 60%.

Table 1 shows a comparison of globally-averaged values of different components of the hydrologic cycle and of the cloud radiative forcing, for January and July. The values represent ensemble averages over the whole observed and simulated period. Note that the time span for the different data sets is not the same. Our integration period agrees with the measuring period from ERBE, but is not the same as the period of observed liquid water path (LWP) from Weng

and Grody (1987-1994), Greenwald et al. (1987-1991) and water vapor mass from Ewald and Schluessel (1987-1988). This might explain some of the differences between model and observations. On a global scale, the only data sets of cloud water/ice content in existence so far are distributions of LWP derived from microwave emissions over ice-free oceans (e.g. Greenwald et al., 1993; Weng and Grody, 1994). However, the accuracy is still rather low, and the retrievals can be affected by many input factors (e.g. total precipitable water, surface wind, precipitation size particles, cloud temperature). Hence, the retrievals from Greenwald et al. and Weng and Grody differ regionally by a factor of two. Therefore we use both data sets as an estimate of the possible range of LWP. Both simulations lie within the observed range, closer to the upper value as retrieved by Greenwald et al. The largest differences between the simulations occur in the ice water path. The total amount in PCI is about 50% higher than that in ECHAM4. The ensemble mean of globally averaged total cloud cover (TCC) in PCI is 64% and 60% for January and July, respectively. It differs insignificantly from the 62% (60%) for January (July) as derived from the International Satellite Cloud Climatology Project (ISCCP; Rossow and Schiffer, 1991) and from surface observations (Hahn et al., 1994). The global means of water vapor mass have slightly increased in PCI as compared to ECHAM4 and to the retrieved values from SSM/I (Ewald and Schluessel, 1995). The seasonal variations and geographical distributions of total precipitation are not that sensitive to changes in the cloud physics. In ECHAM4 53% of the global annual mean total precipitation originates from large-scale clouds, while it is 43% in PCI.

The impact of clouds on the top of the atmosphere (TOA) radiation balance is most conveniently described by the cloud radiative forcing (CF). Following Ramanathan et al. (1989) CF is defined in terms of the emitted longwave radiation F, the solar irradiance S_o, and the albedo α according to:

$$CF = LCF + SCF = (F_{cs} - F) - S_o(\alpha - \alpha_{cs}) \qquad (27)$$

where the subscript cs is used for clear-sky quantities and LCF and SCF represent the longwave and shortwave components of CF, respectively. The global annual mean SCF and LCF in PCI as well as in ECHAM4 have been tuned to match the ERBE data by $\pm 2\,Wm^{-2}$ by an appropriate choice of the microphysical constants which determine the mean lifetime of the clouds (γ_1 to γ_4 in section 2.1). Both simulations show some skill in reproducing the seasonal variations of the shortwave component. Even the largest differences of about $4\,Wm^{-2}$ are probably within the range of observational uncertainty.

3.2. Geographical distribution of cloud water, cloud ice and cloud cover

Figure 2 shows the annual mean latitude-height cross sections of cloud water and cloud ice for ECHAM4 and PCI. For ECHAM4 the separation between water and ice is calculated off-line. The cloud water content has maxima in the lower troposphere associated with tropical shallow convection, and extratropical cyclones in both hemispheres and experiments. Note that one shortcoming of ECHAM4, too high values of cloud water near the surface, is reduced in PCI. Major differences occur in cloud ice. In PCI ice crystals grow rapidly by heterogeneous and contact freezing of cloud droplets.The collection efficiency for snow flakes with ice crystals increases with temperature according to Eq. (23), so that the conversion from ice crystals to snow is faster the warmer the atmosphere is. Therefore maxima in ice water contents are restricted to higher altitudes compared to ECHAM4. In PCI secondary maxima in cloud ice can be seen in the lower troposphere of midlatitudes.

Figures 3 and 4 present the geographical distribution of the LWP for ensemble means of January and July, respectively. Both analyses and model simulations are able to capture the expected maxima in LWP associated with tropical convection and extratropical cyclones in both hemispheres in January and July. In PCI the ECHAM4 overestimation of LWP in convectively active regions, e.g. in the intertropical convergence zone (ITCZ) and the Indian ocean is reduced. Due to high levels of sulfate aerosols and, hence, high concentration of cloud droplets (cf. Fig. 1), LWP is overpredicted offshore the Asian coast in January.

In July the maxima of LWP associated with extratropical cyclones are much more pronounced over northern hemisphere oceans than over southern hemisphere oceans as suggested from SSM/I (Fig. 4). This feature hardly shows up in ECHAM4, but is captured in PCI. Both experiments fail to simulate the dry subsidence region over the western North Pacific. Although stratocumulus decks off the shores of the west coasts of North and South America are suggested in both simulations, their spatial extent is not as large as observed.

Satellite retrievals of cloud ice are not yet available, so the only data sets that can be used for model validation are those obtained during field campaigns (e.g. FIRE, ICE, CEPEX). Figure 5 shows the average ice water content (IWC) versus in-cloud temperature measured by aircraft (Learjet) during the Central Equatorial Pacific Experiment (CEPEX) (Lohmann et al., 1995; McFarquhar and Heymsfield, 1995). Vertical bars indicate the 25% and 75% quartiles of the observations. The simulated IWC of ECHAM4 and PCI within the same domain is taken for the ensembles of March. The average IWC is dominated by a few cases with large IWCs,

because the IWC in each temperature bin is positively skewed. It can, therefore, exceed the 75% percentile value (Fig. 5). Since the Learjet data probably include supercooled cloud droplets, the sum of cloud ice and supercooled cloud water is taken from the model simulations for the comparison. Although the IWC in PCI deviates more from the observed one above 235 K, it still lies between the observed 25% and 75% quartiles. Due to the coarser resolution in the model, extreme values of IWC will hardly appear in the results. The 5% and 95% values in ECHAM4 and PCI have a smaller range than observed. Hence, the variability within each temperature bin is underestimated in both simulations (not shown).

Figures 6 and 7 show the geographical distribution of TCC of ensemble means for January and July, respectively. Note that a very limited amount of data over the oceans is available from the surface observations (Hahn et al. 1994). Both observed data sets agree very well, except over the northern hemisphere continents where the satellite observations tend to underpredict TCC by 10% (Rossow et al., 1993). Maxima in TCC, associated with tropical convection and extratropical cyclones, are captured in both simulations and seasons. In January both simulations underpredict TCC over the northern hemisphere oceans and overpredict it over northern hemisphere continents, even with regard to the surface observations. In July (Figure 7) both simulations underpredict TCC over the stormtracks of the northern hemisphere, but capture high values of TCC associated with the Indian summer monsoon. The Atlantic and Pacific ITCZ which is hardly simulated in ECHAM4 is nicely captured in PCI.

3.3. Geographical distribution of cloud radiative forcing

So far we have discussed the main parameters determining the cloud radiative processes (cloud water, cloud ice and cloud cover). It has been shown that the simulated quantities agree reasonably well with the observed ones. Next the simulated SCF and LCF will be compared to the observed ones from ERBE. Figures 8 and 9 present SCF from ensemble means of January and July, respectively. In January the maximum SCF occurs over southern hemispheric oceans with values up to -200 Wm^{-2}. Secondary maxima are associated with tropical convection. Both simulations capture the overall features but underestimate SCF over southern hemispheric oceans. In July (Fig. 9) the maximum SCF has moved to northern hemispheric oceans following the seasonal cycle of insolation. High values of SCF are also linked to the Indian summer monsoon and to marine stratocumulus decks offshore the Californian coast. ECHAM4 and PCI simulate the gross feature but differ in the details. SCF over the stormtracks is underestimated as a result of underpredicted low-level cloudiness (Chen and Roeckner, 1995). The spatial

extent of secondary maxima associated with marine stratocumulus is too small in both simulations. In both seasons the overestimation of SCF associated with tropical convection is reduced in PCI, which is attributable to the lower values of LWP over convectively active regions. However, SCF is too high over subtropical subsidence oceanic regions.

Finally, ensemble means of LCF for January and July are displayed in Figures 10 and 11, respectively. In contrast to SCF which is mainly determined by the presence of water clouds, LCF is strongly related to the presence of ice clouds. ECHAM4 and PCI simulate the location and seasonal shift of high LCF over the tropics reasonably well. Due to the occurrence of cloud ice in higher altitudes in the extratropics in PCI as compared to ECHAM4, LCF is overestimated poleward of 50^{o} in the winter hemisphere. Instead of one coherent band of convective activity reaching from the Indian ocean via Indonesia to the mid Pacific in January, two distinct centers are simulated in ECHAM4. PCI simulates one coherent band with too low peak values. In July (Fig. 11) ECHAM4 overestimates LCF over the convectively active regions of Indonesia and Central America. In PCI this overprediction is eliminated, but the convective activity in the western Pacific extents too far north. The Pacific ITCZ which is distinctly marked in ERBE is captured in PCI, but interrupted in ECHAM4.

4. Global climate sensitivity

The response of the climate system to a radiative perturbation resulting from, for example, increasing levels of atmospheric CO_2 concentrations depends on a variety of poorly understood feedback mechanisms (IPCC, 1992). One of the most complex and uncertain processes is the cloud-radiation-temperature feedback which involves large but partly compensating changes in the radiative fluxes. In a climate change study Cess et al. (1990) show that even the sign of the feedback varies among the participating GCMs. In this section we analyze the impact of the different cloud schemes on the global climate sensitivity using the same experimental setup and analysis method as in Cess et al. (1990). Climate sensitivity is defined as the TOA radiative response to a global SST forcing which can be regarded as a surrogate climate change. In the reference experiments with ECHAM4 and PCI the climatological July SST is cooled everywhere by 2K, while it is heated by 2K in the respective climate warming experiments. The simulation time of each experiment is 180 days, but the initial spin-up period of 90 days is not considered in the analysis. Following Cess et al. (1990), the climate sensitivity parameter λ is defined as

$$\lambda = (\Delta F/\Delta T_s - \Delta Q/\Delta T_s)^{-1} \tag{28}$$

where ΔT_s is the global mean surface warming and ΔF and ΔQ are the changes of the global mean TOA longwave emission F and net solar radiation Q, respectively. A clear-sky parameter can be defined with the radiative responses ΔF and ΔQ replaced by their respective clear-sky values:

$$\lambda_{cs} = (\Delta F_{cs}/\Delta T_s - \Delta Q_{cs}/\Delta T_s)^{-1} \tag{29}$$

Thus λ/λ_{cs} can be regarded as a measure of cloud feedback with λ/λ_{cs} larger (smaller) 1 denoting a positive (negative) feedback. It was further shown by Cess et al. (1990) that λ/λ_{cs} is proportional to the change in cloud forcing ΔCF:

$$\lambda/\lambda_{cs} = 1 + \Delta CF\,(\Delta F - \Delta Q)^{-1} \tag{30}$$

with CF as defined by Eq. (27). The results are summarized in Table 2.

		ECHAM4	PCI	ECHAM3	GCM Min	Mean	Max
λ_{cs}	[K m^{2}W^{-1}]	0.52	0.48	0.47	0.40	0.47	0.57
λ	[K m^{2}W^{-1}]	0.62	0.48	0.56	0.09	0.65	1.23
λ/λ_{cs}		1.18	1.01	1.18	0.70	1.38	2.47
ΔSCF	[W m^{-2}]	-3.11	0.63	-1.93	-5.9	2.1	7.4
ΔLCF	[W m^{-2}]	4.36	-0.58	3.25	-4.2	-0.5	3.0
ΔCF	[W m^{-2}]	1.25	0.05	1.32	-2.9	1.6	5.1
ΔTCC	[%]	1.42	-2.44	-1.19	-4.4	-2.1	-0.2
ΔTWP	[g m^{-2}]	12.8	6.8	10.9			

Table 2: Global mean sensitivity parameters for the total atmosphere surface system, including cloud effects (λ), and for clear-sky reference atmosphere (λ_{cs}). λ/λ_{cs} and ΔCF are measures of cloud feedback. ΔSCF and ΔLCF denote the shortwave and longwave components of ΔCF. ΔTCC is the change in total cloud cover and ΔTWP in total cloud water (liquid+ice) path. The respective parameters (minimum, mean and maximum) obtained in a GCM intercomparison study by Cess et al. (1990) and the values obtained from a previous version of ECHAM (Lohmann and Roeckner, 1995) are shown in addition.

The clear-sky sensitivity parameter λ_{cs} is similar in all three experiments and falls into the range of model sensitivities analyzed by Cess et al. (1990). The deviations among the experiments are larger in the global feedback parameter λ. Largest differences occur in the individual components of the change in CF. The feedback λ/λ_{cs} and the individual components of ECHAM4 are qualitatively similar to the ones of ECHAM3 (Lohmann and Roeckner, 1995), and will only be briefly summarized. Clouds enhance the global sensitivity by nearly 20%, therefore the cloud feedback is positive. Water and ice clouds have been lifted into higher altitudes in the warmer atmosphere and their contents have increased by 9.8 g m^{-2} and 3 g m^{-2}. This is particularly relevant for nonblack cirrus, because its emissivity increases as the ice content increases. Thus LCF has increased by 4.4 Wm^{-2}. ΔSCF is negative (-3.1 Wm^{-2}) caused by the increase in TWP and optical depth resulting in a higher cloud albedo. The changes in LCF and SCF are larger than in ECHAM3 probably due to different radiation schemes and, hence, different cloud optical properties.

In PCI the cloud feedback is zero. The changes in SCF and LCF are smaller and of opposite sign as in ECHAM3 and ECHAM4. Both changes are in phase with the mean of model sensi-

tivities analyzed by Cess et al. (1990). In PCI the decrease in total water path is only half of that in ECHAM in which the ice water path actually decreases by 8%. It is probably caused by the faster accretion of snow with ice in the warmer atmosphere (cf. Eq. (23)). It also corresponds to the findings of Fig. 5, that the slope of supercooled cloud water and cloud ice with temperature in PCI is not as steep as in ECHAM4 and, thus, fits better to the observations. The decrease in cloud ice leads to a reduction in LCF. The smaller SCF in the warmer climate is caused by the decrease in low level clouds. Lohmann and Roeckner (1995) argue that the radiative impact of clouds is probably overestimated in ECHAM, because microphysical parameters, like droplet concentration or size spectrum are neglected. Analyses of ground-based lidar/radiometer and in situ aircraft measurements of cloud properties (Platt, 1989) suggest that the cirrus emissivity is actually less sensitive to a change in temperature than the cloud water content, because the particle size is positively correlated with temperature as well (cf. also Ou and Liou, 1995). For warm continental and almost all maritime clouds even a negative correlation between temperature and optical depth has been derived from ISCCP (Tselioudis, 1992). Therefore the zero feedback with the more advanced cloud scheme is not that surprisingly.

Even though the cloud feedback differs in ECHAM4 and PCI, the geographical pattern of the change in temperature, cloud cover or zonal wind are similar. Mid level clouds are reduced and high level clouds increased as a result of tropopause lifting in the warmer climate in both experiments (not shown). However, the changes in temperature, wind and stream function are smaller in PCI. This could be due to the different changes in longwave cloud forcing (+4.4 Wm^{-2} in ECHAM4, -0.6 Wm^{-2} in PCI). Model results indicate that the infrared cloud-radiative warming, although considerable smaller than the latent heat release in convective clouds, has a crucial influence on the atmospheric circulation (e.g. Slingo and Slingo, 1988; Randall et al., 1989; Sherwood et al., 1994). The absence of the longwave cloud forcing can weaken the Walker circulation by 50% (Lohmann and Roeckner, 1995). Figure 12 shows the latitude-pressure cross section of the change in zonal mean zonal wind between the SST+2K and the SST-2K experiment. The maximum increase in wind speed in the warmer climate is about twice as large in ECHAM4 as in PCI. Additionally the increase in wind speed is not restricted to high altitudes in ECHAM4.

To summarize, our simulated results indicate that the temperature dependence of cloud water/ice and the level of parameterization of cloud microphysics is crucial for the cloud-temperature-radiation feedback. While cloud water/ice increases more rapidly with temperature in ECHAM4 and ECHAM3 resulting in a positive cloud feedback, the weaker increase in PCI

yields a zero cloud feedback.

5. Summary and Conclusions

First results obtained from a prognostic cloud ice scheme (PCI) in the general circulation model ECHAM are presented. In contrast to the standard scheme of ECHAM4, the autoconversion from cloud water to rain depends additionally on the cloud droplet number concentration (N_l) to account for the different microphysical properties of maritime and continental clouds (Beheng, 1994). N_l is empirically related to the sulfate aerosol mass (Boucher and Lohmann, 1995). Similarly the aggregation of ice crystals to snow depends additionally on the ice crystal size (Levkov et al., 1992), which in turn is a function of the ice content (Moss et al., 1995). The vertical distribution of cloud ice differs remarkably between the two schemes. While ECHAM4 always assumes mixed clouds between -40°C and -0°C, in PCI supercooled water clouds can exist down to -35°C and pure ice clouds up to 0°C. Once glaciation of these clouds starts, the subsequent precipitation formation is more efficient for larger ice crystals. Additionally the accretion of snow flakes with ice crystals is more efficient for higher temperatures. Therefore maxima in ice content in PCI are confined to higher altitudes and the ice water path is roughly 50% higher than in ECHAM4.

In general, the simulated distribution of the liquid and ice water content with ECHAM4 and with PCI are within the range of the observational uncertainty which is unfortunately very high. The climatology of cloud physical and radiative properties is reasonably well simulated with ECHAM4. Therefore only minor improvements are achieved with PCI, e.g. the overestimation of the liquid water path (LWP) in convectively active regions is reduced. However, some shortcoming like the overprediction of LWP off the shores of the Asian coast due to high values of N_l occur. Here we have taken a simple empirical approach to relate N_l to the monthly mean values of sulfate aerosol mass. However, as discussed in Boucher and Lohmann (1995), other aerosol components like nitrate or organic species also act as cloud condensation nuclei and form cloud droplets. Furthermore, a realistic aerosol size distribution should be considered. Thus, a future project would be to couple N_l to aerosol physics as developed by Keup-Thiel (1995) for a chemical transport model.

Chen and Roeckner (1995) conclude that the large shortwave cloud forcing (SCF) in ECHAM4 in the tropics results most likely from the neglect of cloud inhomogeneities and not from the overestimation of LWP. In contrast to that, the zonal mean LWP is reduced in the

tropics up to 15% in July in PCI as compared to ECHAM4 and, thus, SCF is reduced by the same percentage. The shortwave albedo bias as observed from stratocumulus clouds in FIRE resulting from the neglect of cloud inhomogeneities can be as large as 15% (Calahan et al., 1994). However, Joseph and Zackhem (1995) show that internal cloud inhomogeneities and that of an individual cloud itself can oppose each other and level the albedo bias. With respect to the LWP retrieval from Greenwald et al. (1993) one could argue that LWP in the subtropics in both simulations is not overestimated but SCF is too high, which must, therefore, be due to cloud inhomogeneities. On the other hand LWP in the subtropics is too high compared to the retrieval of Weng and Grody (1994), and, consequently SCF is overpredicted. Thus more observations of LWP as well as more knowledge about three dimensional cloud inhomogeneities are needed before one reasonably can account for cloud inhomogeneities in GCMs.

One motivation for improving the cloud microphysics scheme is the large uncertainty of the role of clouds in global warming experiments. The global cloud feedback defined according to Cess et al. (1990) is positive in ECHAM3 and ECHAM4, but is zero in PCI. In particular the changes of the longwave and shortwave component of the cloud forcing are of opposite sign in PCI as compared to ECHAM4. In ECHAM4 the large increase in total water path yields a higher LCF and SCF in the warmer climate. Reversely the decrease in ice water path and cloud cover in PCI reduces LCF and SCF in the warmer climate and yields a zero cloud radiation feedback.

Acknowledgments

We thank T. Greenwald and F. Grody for providing the SSM/I cloud water data. We also thank A. Chlond and L. Levkov for useful discussions.

References

Albrecht BA (1989) Aerosols, cloud microphysics, and fractional cloudiness. Science 245: 1227-1230

Arakawa A (1975) Modelling clouds and cloud processes for use in climate models. GARP Publication Series No. 16, ICSU/WMO: 183-197

Beheng KD (1994) A parameterization of warm cloud microphysical conversion processes. Atmos. Res. 33: 193-206

Berry EH, RL Reinhardt, 1973: Modeling of condensation and collection within clouds, D.R.I. Phys. Sci. Pub. 16, University of Nevada.

Bigg EK (1953) The supercooling of water. Proc. Phys. Soc. 66: 688-694

Boer GJ, NA McFarlane, R Laprise, JD Henderson, JP Blanchet (1984) The Canadian Climate Center spectral atmospheric circulation model. Atmosphere-Ocean 22: 397-429

Boucher O, H Le Treut, MB Baker (1995) Precipitation and radiation modelling in a GCM: Introduction of cloud microphysical processes. Subm. to J. Geophys. Res.

Boucher O, U Lohmann (1995) The sulfate-CCN-cloud albedo effect. A sensitivity study with two general circulation models. Tellus 47B: 281-300

Brinkop S, E Roeckner (1995) Sensitivity of a general circulation model to parameterizations of cloud-turbulence interactions in the atmospheric boundary layer. Tellus 47A: 197-220

Calahan RF, W Ridgway, WJ Wiscombe, TL Bell (1994) The albedo of stratocumulus clouds. J. Atmos. Sci. 51: 2434-2455

Cess RD, GL Potter, JP Blanchet, GJ Boer, AD Del Genio, M Deque, V Dymnikov, V Galin, WL Gates, SJ Ghan, JT Kiehl, AA Lacis, H Le Treut, ZX Li, XZ Liang, BJ McAvaney, VP Meleshko, JFB Mitchell, JJ Morcrette, DA Randall, L Rikus, E Roeckner, JF Royer, U Schlese, DA Sheinin, A Slingo, AP Sokolov, KE Taylor, MW Washington, RT Wetherald, I Yanai, MH Zhang (1990) Intercomparison and interpretation of climate feedback processes in 19 atmospheric general circulation models. J. Geophys. Res. 95: 16601-16615

Chen C, WR Cotton (1987) The physics of the marine stratocumulus-capped mixed layer. J. Atmos. Sci. 44: 2951-2977

Chen CT, E. Roeckner, 1995: Validation of the Earth radiation budget as simulated by the Max Planck Institute for Meteorology general circulation model ECHAM4 using satellite observations of the Earth Radiation Budget Experiment (ERBE). Subm. to J. Geophys. Res.

Claussen M, U Lohmann, E Roeckner, U Schulzweida (1994) A global data set of land-surface parameters. Report No. 135, Max-Planck-Institut für Meteorologie, Germany, 23pp

Collins WD, WC Conant, V Ramanathan (1994) Earth radiation budget, clouds and climate sensitivity. In: The chemistry of the atmosphere: Its impact on global change, edited by JG Calvert, Oxford, UK.: 207-215

Cotton WR, GJ Tripoli, RM Rauber and EA Muluihili (1986) Numerical simulation of the effects of varying ice crystal nucleation rates and aggregation processes on orographic snowfall, J. Climate Appl. Meteorol. 25: 1658-1680

Del Genio AD, MS Yao, W Kovari, KKW Lo (1995) A prognostic cloud water parameterization for global climate models. J. Climate, in press.

Eppel DP, H Kapitzka, M Claussen, D Jacob, W Koch, L Levkov, HT Mengelkamp, N Werrmann (1995) The non-hydrostatic mesoscale model GESIMA. Part II: Parameterizations and applications. Beitr. Phys. Atm. 68: 15-41

Ewald S, P Schluessel (1995) Hydrologic parameters from SSM/I data. Manuscript in preparation.

Feichter J, E Kjellström, H Rodhe, F Dentener, J Lelieveld, GJ Roelofs (1995) Simulation of the tropospheric sulfur cycle in a global climate model. Atm. Env., in press.

Fouquart Y, B Bonnel (1980) Computations of solar heating of the Earth's atmosphere: A new parameterization. Beitr. Phys. Atmos. 53: 35-62

Fouquart Y, H Isaka (1992) Sulfur emission, CCN, clouds and climate: a review. Ann Geophysicae 10: 462-471

Fowler LD, DA Randall, SA Rutlegde (1995) Liquid and ice cloud microphysics in the CSU general circulation model. Part I: Model description and simulated microphysical processes. J. Climate, in press.

Gates WL (1992) AMIP: The atmospheric model intercomparison project. Bull. Amer. Meteor. Soc. 73: 1962-1970

Geleyn JF (1981) Some diagnostics of the cloud radiation interaction on ECMWF forecasting model. In: Workshop on radiation and cloud-radiation interaction in numerical modelling. 15-17.Oct. 1980, ECMWF, Reading: UK, 135-162

Ghan SJ, RC Easter (1992) Computationally efficient approximations to stratiform cloud microphysics parameterization. Mon. Wea. Rev. 120: 1572-1582

Greenwald TJ, GL Stephens, TH Vonder Haar, DL Jackson (1993) A physical retrieval of cloud liquid water over the global oceans using Special Sensor Microwave/Imager (SSM/I) observations. J. Geophys. Res. 98: 18471-18488

Gunn KLS, JS Marshall (1958) The distribution with size of aggregate snowflakes. J. Meteor.

15: 452-461

Hahn CJ, SG Warren, J London (1994) Climatological data for clouds over the globe from surface observations, 1982-1991: The total cloud edition, ORNL/CDIAC-72, NDP-026A, Oak Ridge National Laboratory, Oak Ridge, Tennessee, USA

Heymsfield AJ, CMR Platt (1984) A parameterization of the particle size spectrum of ice clouds in terms of the ambient temperature and the ice water content. J. Atmos. Sci. 41: 846-855

IPCC, Climate Change (1992) The supplementary report to the IPCC scientific assessment, 200 pp., edited by JT Houghton, BA Callander, S K Varney. Cambridge University Press, Cambridge, UK

Johnson DW (1993) Parameterisation of the cloud topped boundary layer. Aircraft measurements. ECMWF Workshop Proceedings 'Parameterization of the cloud topped boundary layer', 77-117, European Centre for Medium-Range Weather Forecasts, Reading, UK

Joseph JH, U Zackhem (1995) Flux radiative transfer through a cloudy layer. IUGG XXI General Assembly, Boulder, 2.-14.7.1995, B266

Kessler E (1969) On the distribution and continuity of water substance in atmospheric circulations, Meteor. Mono., 32, Amer. Meteor. Soc., 84pp.

Keup-Thiel E (1995) The Aerosol Particle Module (APMO) for calculations of global aerosol distributions. In: Proceedings from the Third International Conference on Modelling Climate Change and Variability. 4-8 Sept. 1995, Hamburg, Germany

Kiehl JT, JJ Hack, BP Briegleb (1994) The simulated Earth radiation budget of the National Center for Atmospheric Research community climate model CCM2 and comparisons with the Earth Radiation Budget Experiment (ERBE) J. Geophys. Res. 99: 20815-20827

King MD, LF Radke, PV Hobbs (1993) Optical properties of marine stratocumulus clouds modified by ships. J. Geophys. Res. 98: 2729-2739

Lee JL, KN Liou, SC Ou (1992) A three-dimensional large-scale cloud model: Testing the role of radiative heating and ice phase processes. Tellus, 44A: 197-216

Le Treut H, ZX Li (1988) Using Meatiest data to validate a prognostic cloud generation scheme. Atmos. Res. 21: 273-292

Levkov L, B Rockel, H Kapitza, E Raschke (1992) 3D mesoscale numerical studies of cirrus and stratus clouds by their time and space evolution. Beitr. Phys. Atmos. 65: 35-58

Lin YL, RD Farley, HD Orville (1983) Bulk parameterization of the snow field in a cloud model. J. Cli. Appl. Meteor., 22: 1065-1092

Lohmann U, E Roeckner (1995) Influence of cirrus cloud radiative forcing on climate and climate sensitivity in a general circulation model. J. Geophys. Res. 100: 16305-16323

Lohmann U, E Roeckner, WD Collins, AJ Heymsfield, GM McFarquhar, TP Barnett (1995) The role of water vapor and convection during the Central Equatorial Pacific Experiment (CEPEX) from observations and model simulations. J. Geophys. Res., in press.

Lord SJ, HE Willoughby, JM Piotrowicz (1984) Role of parameterized ice-phase microphysics in an axialsymmetric, nonhydrostatic tropical cyclone model. J. Atmos. Sci. 41: 2836-2848

Manabe S, J Smagorinsky, RF Strickler (1965) Simulated climatology of a general circulation model with a hydrological cycle. Mon. Wea. Rev. 93: 769-798

Mason BJ (1971) The physics of clouds. Clarendon Press, Oxford, 671 pp

Matveev LT (1984) Cloud dynamics; Atm. Sci. Library, D. Reidel Publishing Company, Dordrecht, 340 pp

McFarlane NA, GJ Boer, JP Blanchet, M Lazare (1992) The Canadian Climate Centre second-generation general circulation model and its equilibrium climate. J. Climate: 1013-1044

McFarquhar GM, AJ Heymsfield (1995) In-situ observations of the horizontal and vertical structure of three cirrus anvils sampled during the Central Equatorial Pacific Experiment (CEPEX). Subm. to J. Atmos. Sci.

Mitchell JFB, CA Senior, WJ Ingram (1989) CO_2 and climate: A missing feedback? Nature 341: 132-134

Mölders N, M Laube, G Kramm (1994) A scheme for parameterizing ice and water clouds in regional models. A contribution to subproject EUMAC

Morcrette JJ (1991) Radiation and cloud radiative properties in the European Centre for Medium Range Weather Forecasts forecasting system. J. Geophys. Res., 96: 9121-9132

Moss SJ, PN Francis, DW Johnson, D Percival (1995) The calculation and parameterisation of the effective radius of ice particles using aircraft data. Subm. to Q. J. R.Meteorol. Soc.

Murakami M (1990) Numerical modeling of dynamical and microphysical evolution of an isolated convective cloud - The 19 July 1981 CCOPE cloud. J. Meteor. Soc. Japan 68: 107-128

Nordeng TE (1995) Extended versions of the convective parameterization scheme at ECMWF and their impact on the mean and transient activity of the model in the tropics. Subm. to Q. J. R. Meteorol. Soc.

Ose T (1993) An examination of the effects of explicit cloud water in the UCLA GCM. J. Meteor. Soc. Japan 71: 93-109

Ou SC, KN Liou (1995) Ice microphysics and climatic temperature feedback. Atmos. Res. 35:

127-138

Platt CMR (1989) The role of cloud microphysics in high-cloud feedback effects on climate change. Nature 341: 428-429

Potter BE (1991) Improvements to a commonly used cloud microphysical bulk parameterization. J. Appl. Meteor. 30, 1040-1042

Pruppacher HR, JD Klett (1978) Microphysics of clouds and precipitation. D. Reidel, 714pp.

Radke LF, JA Coagley Jr., MD King (1989) Direct and remote sensing observations of the effects of ships on clouds. Science 246: 1146-1149

Ramanathan V, RD Cess, EF Harrison, P Minnis, BR Barkstrom E Ahmad, D Hartmann (1989) Cloud-radiative forcing and climate: Results from the Earth Radiation Budget Experiment. Science 243: 57-63

Randall DA, Harshvardhan, DA Dazlich, TG Corsetti (1989) Interactions among radiation, convection and large-scale dynamics in a general circulation model. J. Atmos. Sci. 46: 1943-1970

Rangno AL, PV Hobbs (1994) Ice particle concentrations and precipitation development in small continental cumuliform clouds. Q. J. R. Meteorol. Soc. 120: 573-601

Rasch PJ, DL Williamson (1990) Computational aspects of moisture transport in global models of the atmosphere. Q. J. R. Meteorol. Soc. 116: 1071-1090

Rockel B, E Raschke, B Weyres (1991) A parameterization of broad band radiative transfer properties of water, ice and mixed clouds. Beitr. Phys. Atmos. 64: 1-12

Roeckner E, U Schlese (1985) January simulation of clouds with a prognostic cloud cover scheme; ECMWF Workshop on "Cloud cover in numerical models", 26-28 Nov. 1984, 87-108, ECMWF, Reading, UK

Roeckner E, K Arpe, L Bengtsson, S Brinkop, L Dümenil, M Esch, E Kirk, F Lunkeit, M Ponater, B Rockel, R Sausen, U Schlese, S Schubert, M Windelband (1992) Simulation of the present-day climate with the ECHAM model: Impact of model physics and resolution. Report No. 93, Max-Planck-Institut für Meteorologie, Germany, 172 pp

Rossow WB, RA Schiffer (1991) ISCCP cloud products. Bull. Amer. Soc. 72: 2-20

Rossow WB, AW Walker, LC Garder (1993) Comparison of ISCCP and other cloud amounts. J. Climate 6: 2394-2418

Rutledge SA, PV Hobbs (1983) The mesoscale and microscale structure and organization of clouds and precipitation in midlatitude cyclones. VII: A model for the "Seeder Feeder" process in warm-frontal bands. J. Atmos. Sci. 40: 1185-1206

Sherwood SC, V Ramanathan, TP Barnett, MK Tyree, E Roeckner (1994) Response of an atmospheric GCM to radiative forcing of tropical clouds. J. Geophys. Res. 99: 20829-20845

Slingo JM (1987) The development and verification of a cloud prediction scheme for the ECMWF model. Q. J. R. Meteorol. Soc. 113: 899-927

Slingo A, JM Slingo (1988) The response of a general circulation model to cloud longwave radiative forcing. I. Introduction and initial experiments. Quart. J. R. Met. Soc. 114: 1027-1062

Smith RN (1990) A scheme for predicting layer clouds and their water content in a general circulation model. Q. J. R. Meteorol. Soc. 116: 435-460

Sundqvist H (1978) A parameterization scheme for non-convective condensation including prediction of cloud water content. Q. J. R. Meteorol. Soc. 104: 677-690

Sundqvist H, E Berge, JE Kristjansson (1989) Condensation and cloud parameterization studies with a mesoscale numerical weather prediction model. Mon. Wea. Rev., 117: 1641-1657

Tiedtke M (1989) A comprehensive mass flux scheme for cumulus parameterization in large-scale models. Mon. Wea. Rev. 121: 3040-3061

Tselioudis G, WB Rossow, D Rind (1992) Global patterns of cloud optical thickness variation with temperature. J. Climate 5: 1484-1495

Weng F, NC Grody (1994) Retrieval of cloud liquid water using the special sensor microwave imager (SSM/I). J. Geophys. Res. 99: 25535-25551

Xu KM, SK Krueger (1991) Evaluation of cloudiness parameterizations using a cumulus ensemble model. Mon. Wea. Rev. 119: 342-367

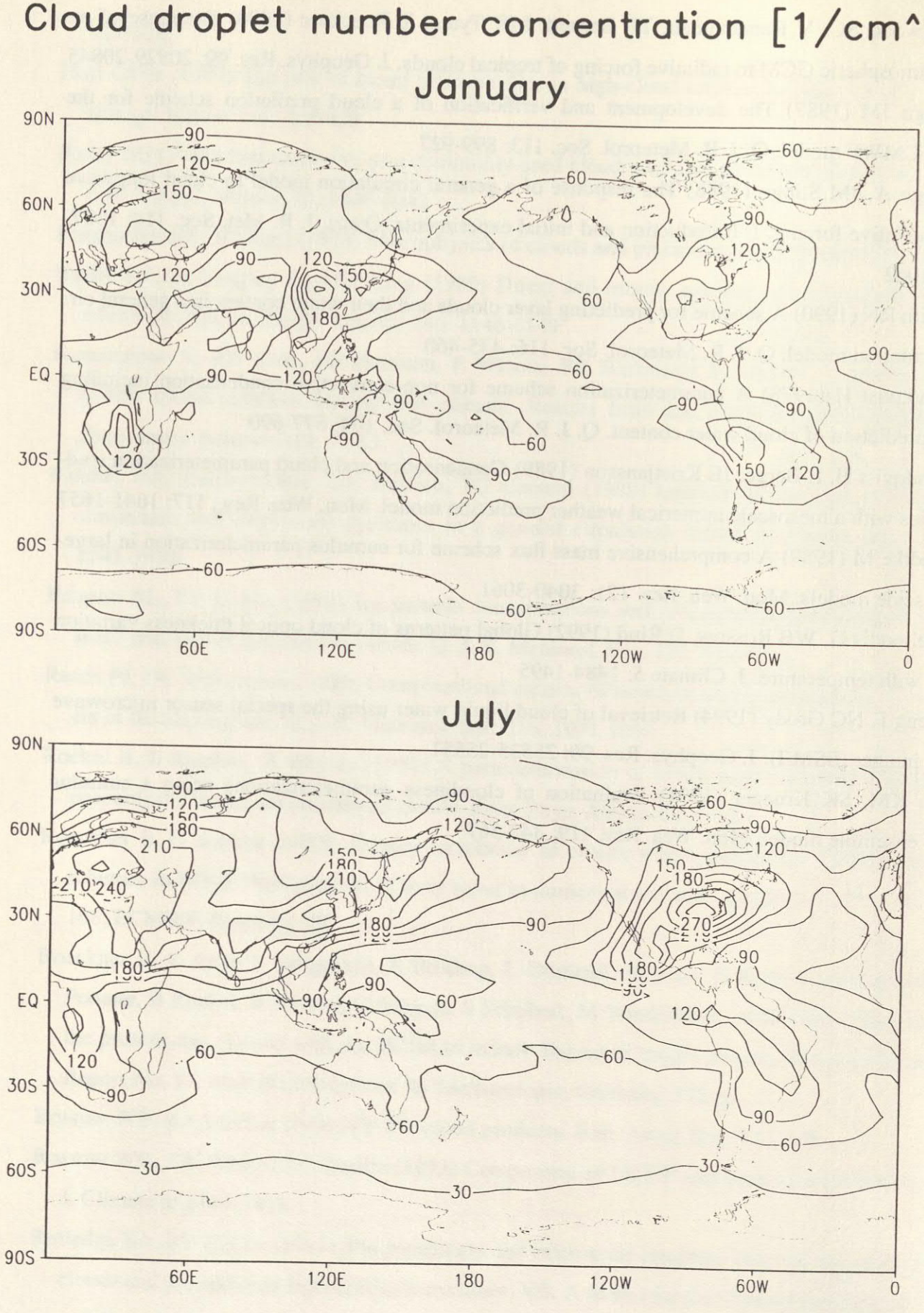

Figure 1: Cloud droplet number concentration [1cm^{-3}] for January (upper panel) and July (lower panel).

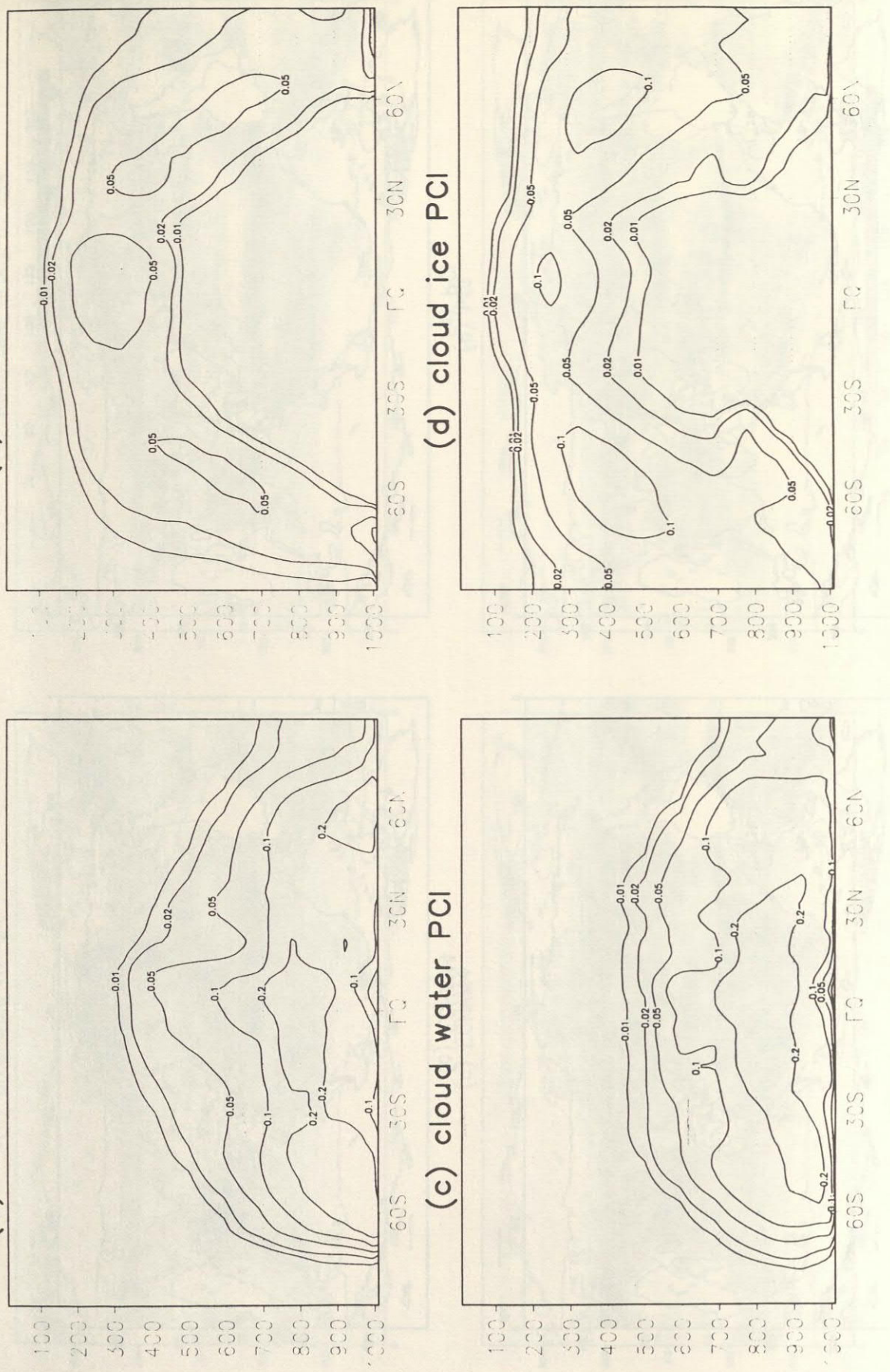

Figure 2: Annual mean latitude-height cross sections of cloud water and cloud ice [10^{-4} kg kg^{-1}] for ECHAM4 (a,b) and PCI (c,d), respectively.

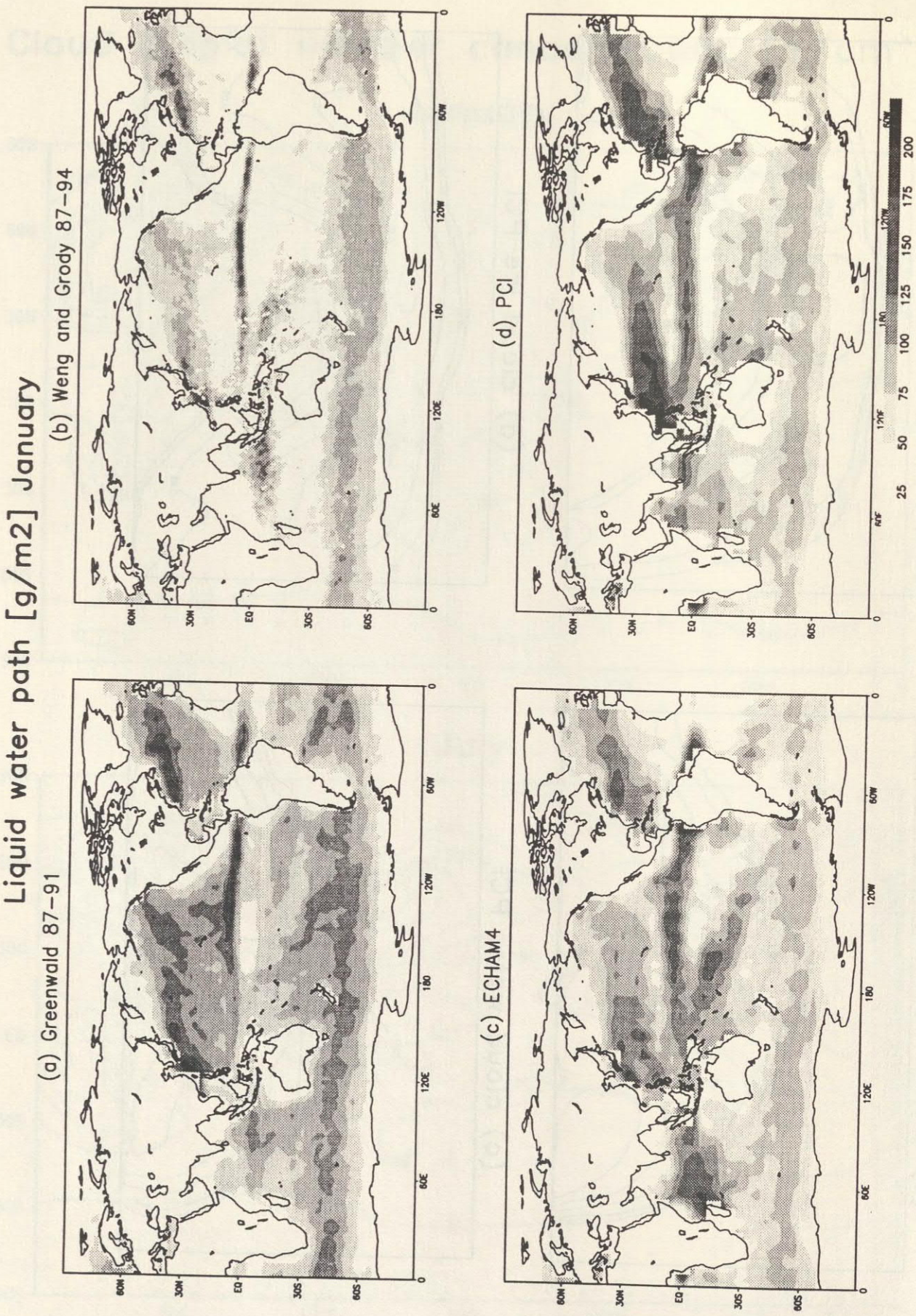

Figure 3: Geographical distribution of liquid water path [g m^{-2}] for January obtained from a) SSM/I analyses according to Greenwald et al. (1993) (a), SSM/I analyses according to Weng and Grody (1994) (b), ECHAM4 (c) and PCI (d).

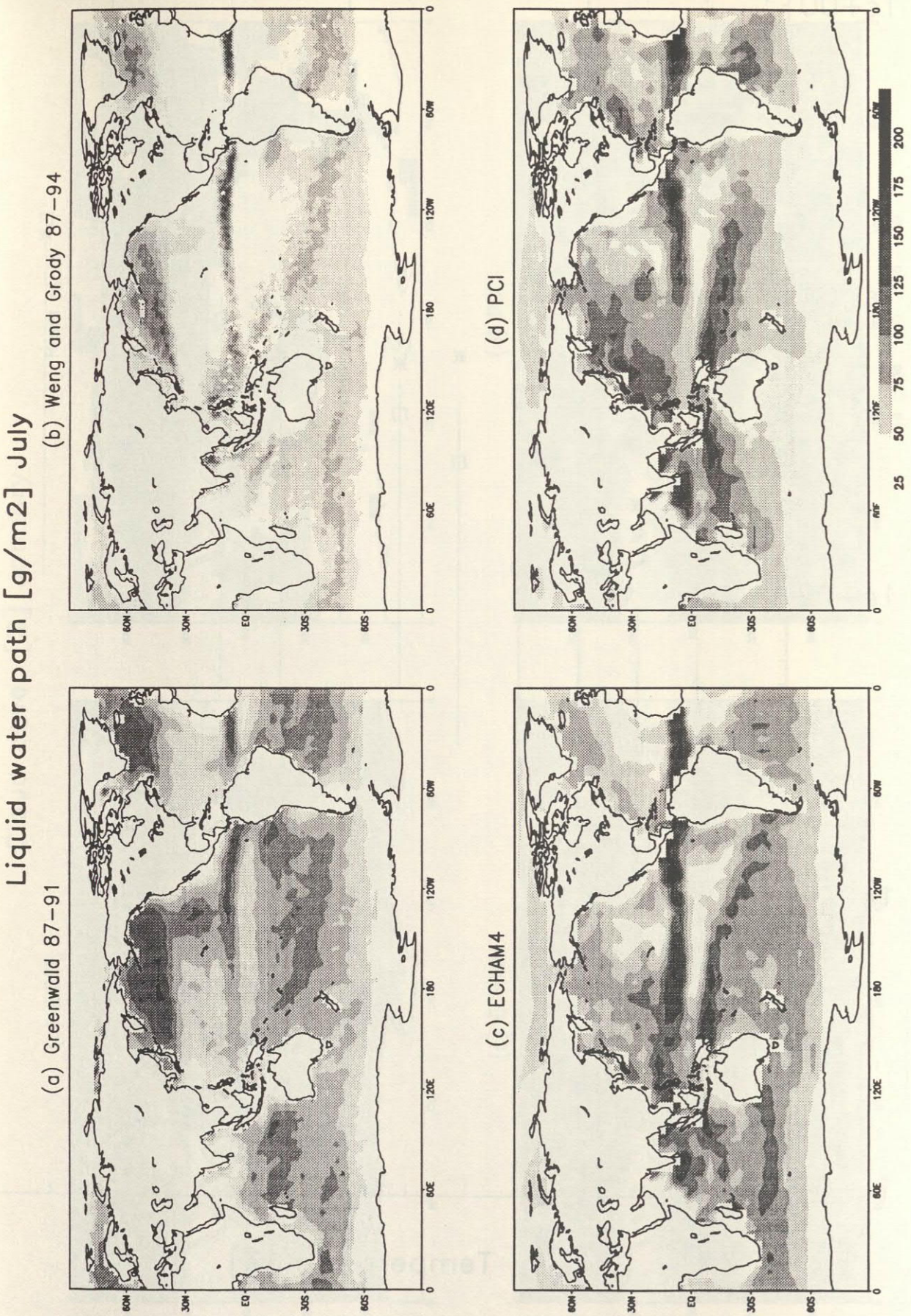

Figure 4: As Figure 3 except for July.

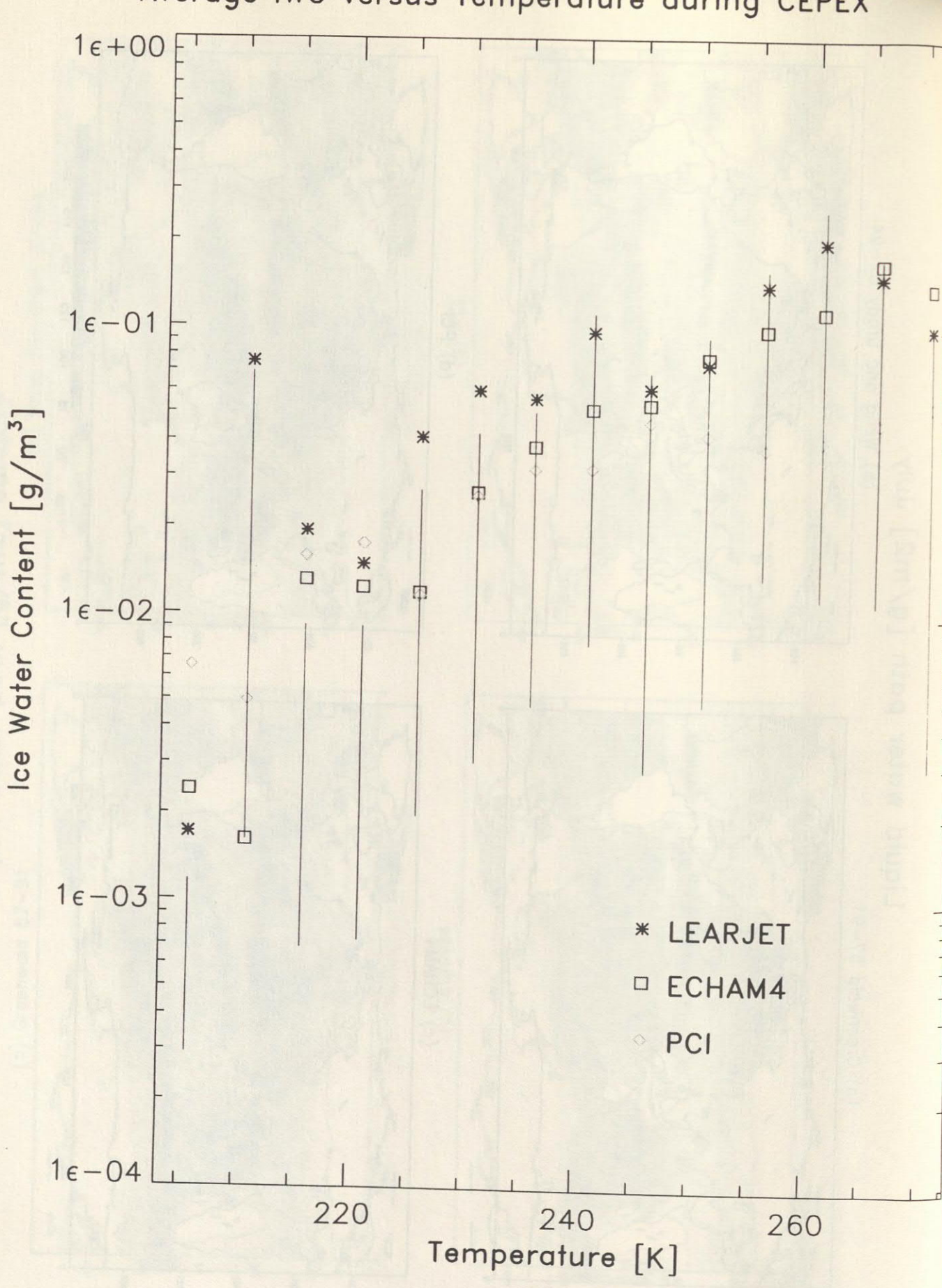

Figure 5: Mean ice water content versus in-cloud temperature in 5K temperature bins from 2DC-probe data carried on the Aeromet Learjet (stars) during CEPEX as compared to ECHAM4 (squares) and PCI (rhombs). Vertical bars represent the 25% and 75% quartiles from the Learjet data.

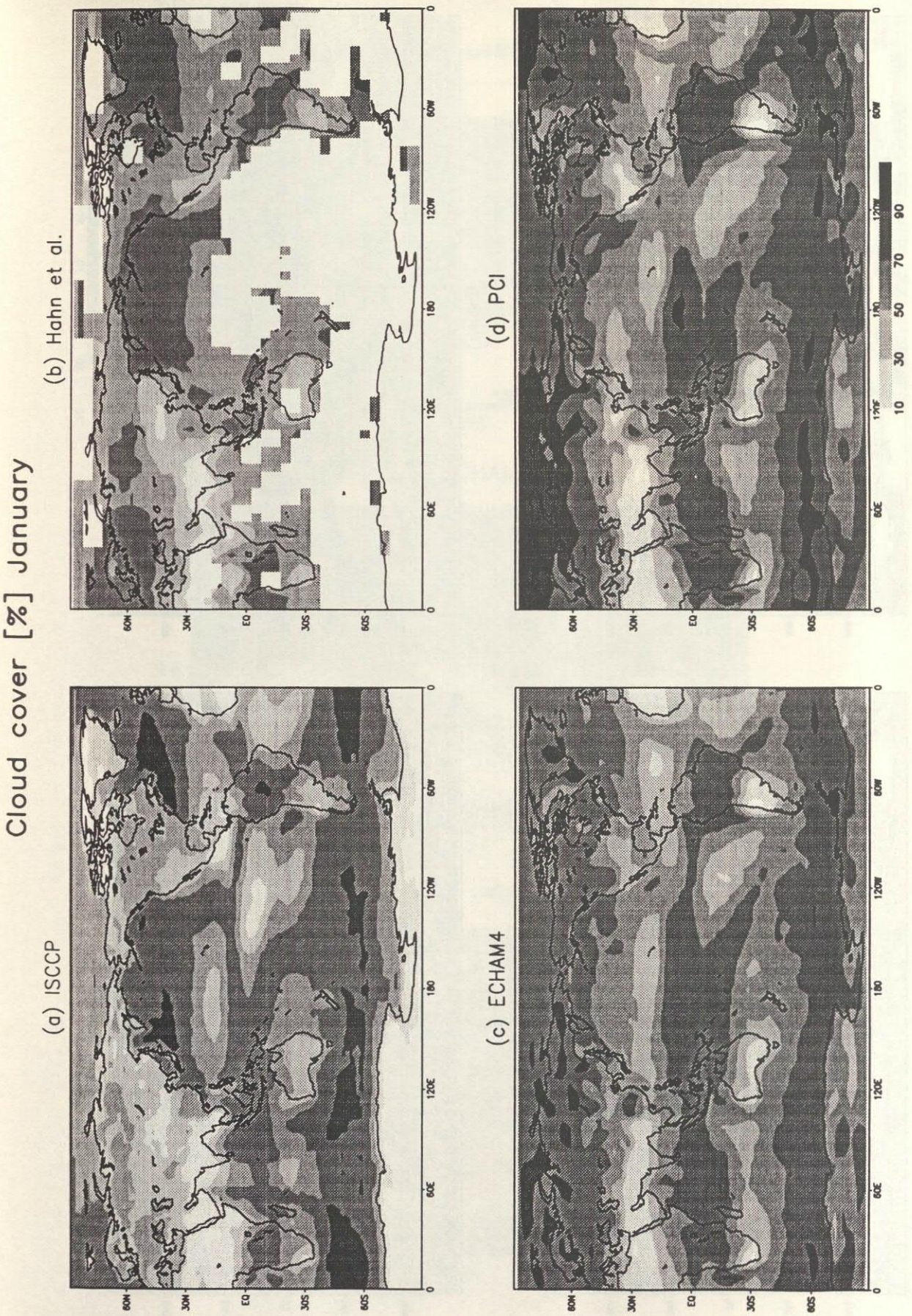

Figure 6: Geographical distribution of cloud cover [%] for January obtained from ISCCP (a), surface observations (Hahn et al. 1994) (b), ECHAM4 (c) and PCI (d).

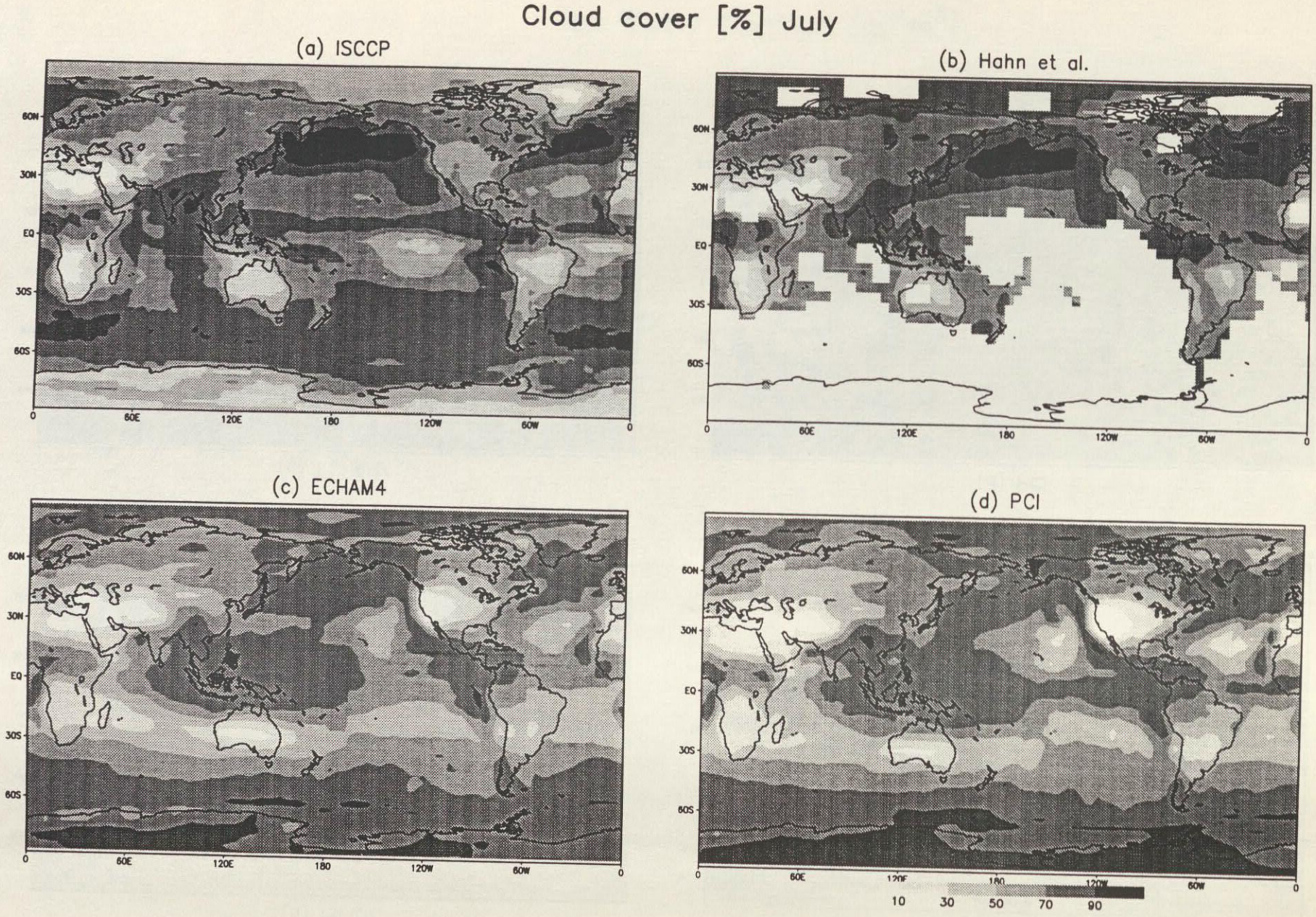

Figure 7: As Figure 6 except for July.

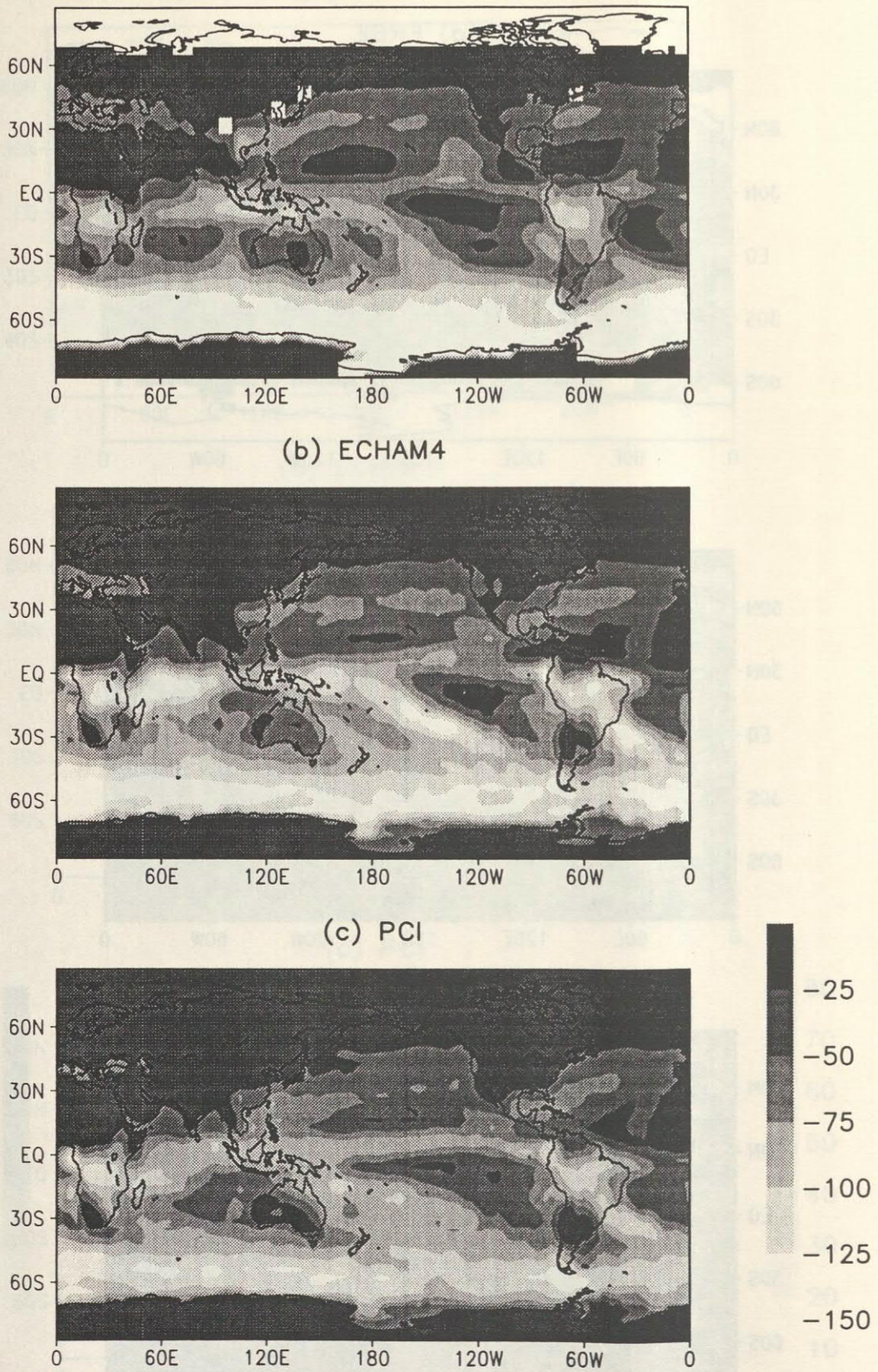

Figure 8: Geographical distribution of shortwave cloud forcing [Wm^{-2}] for January obtained from ERBE (a), ECHAM4 (b) and PCI (c).

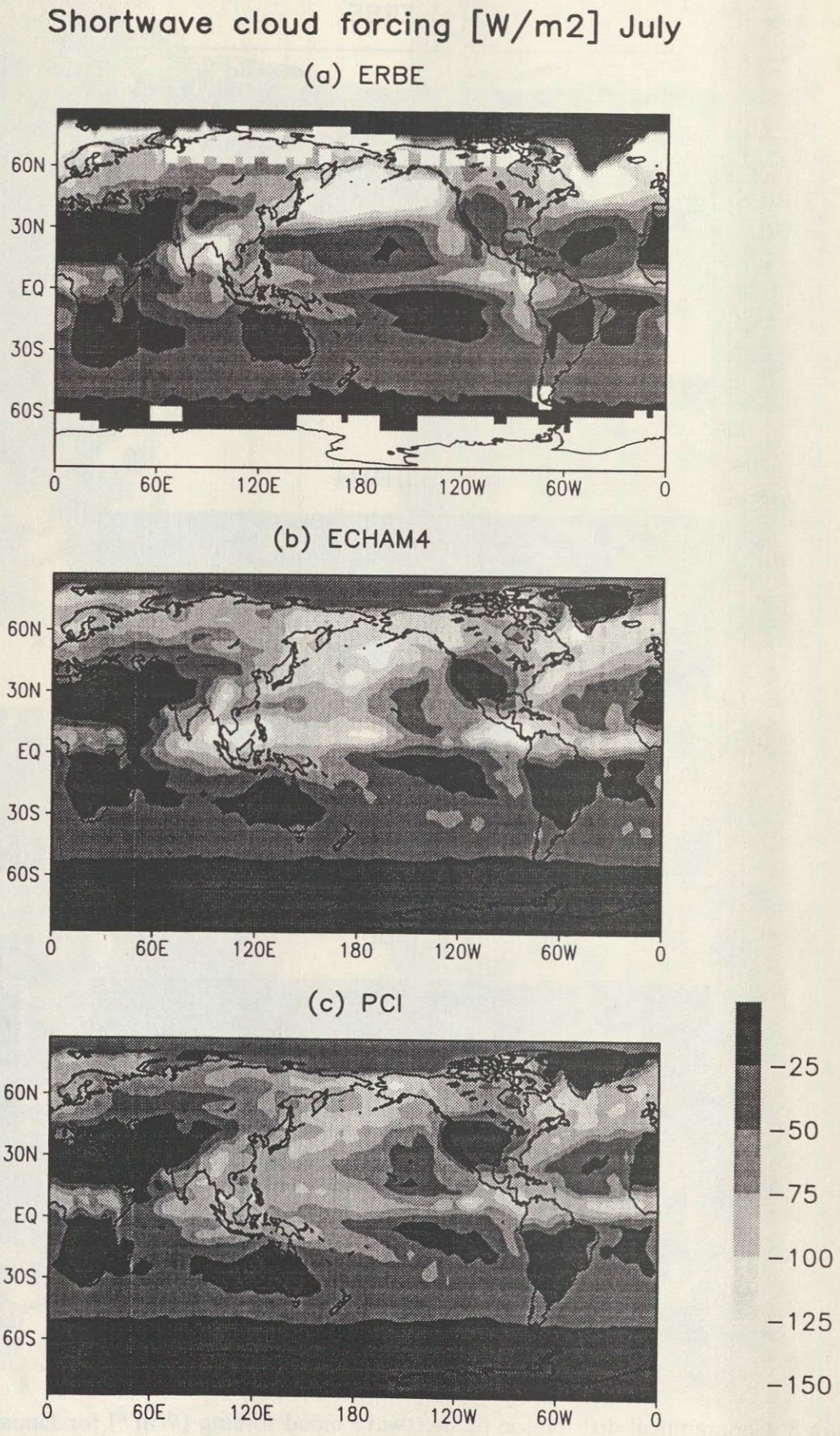

Figure 9: As Figure 8 except for July.

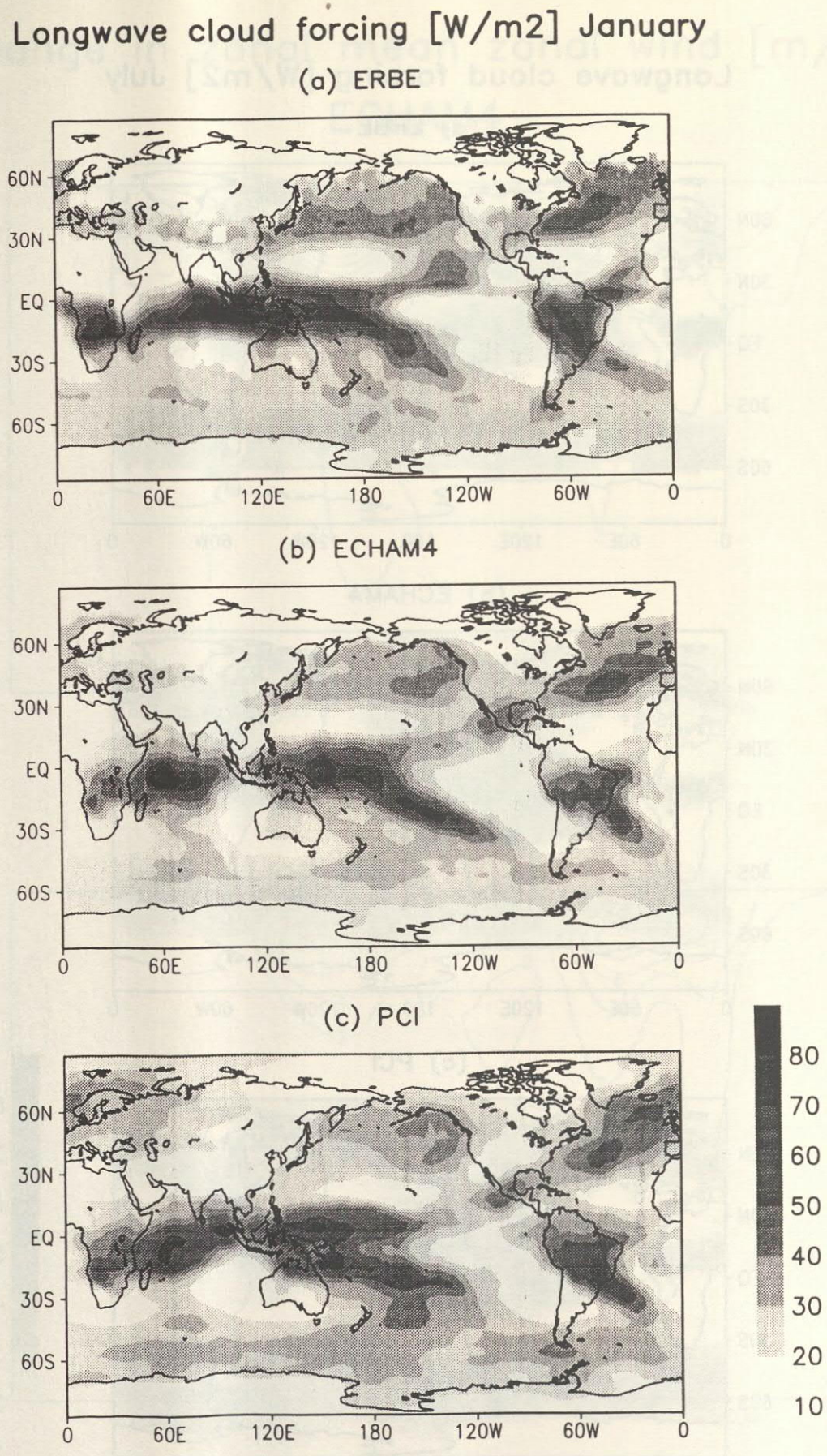

Figure 10: Geographical distribution of longwave cloud forcing [Wm^{-2}] for January obtained from ERBE (a), ECHAM4 (b) and PCI (c).

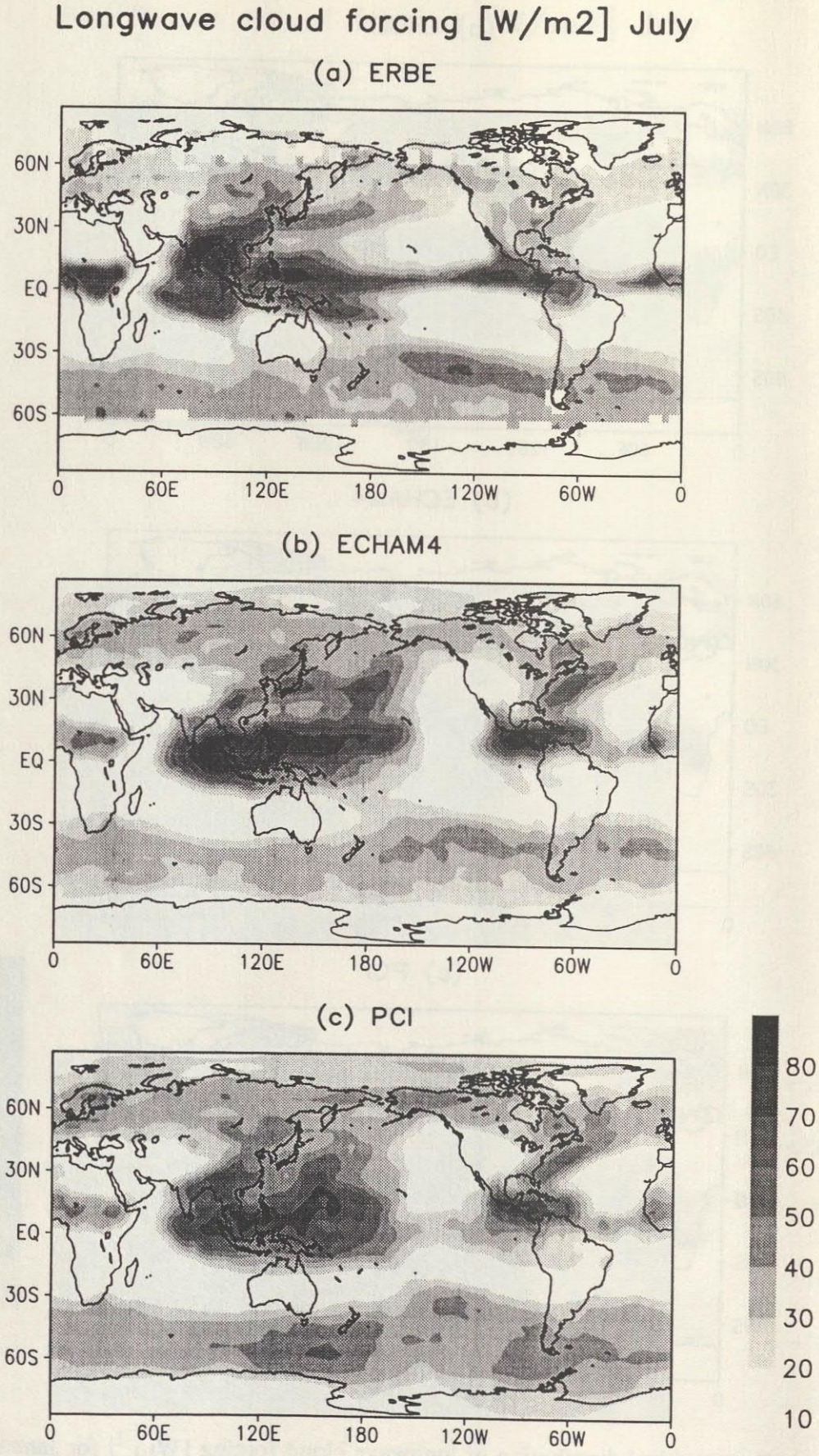

Figure 11: As Figure 10 except for July.

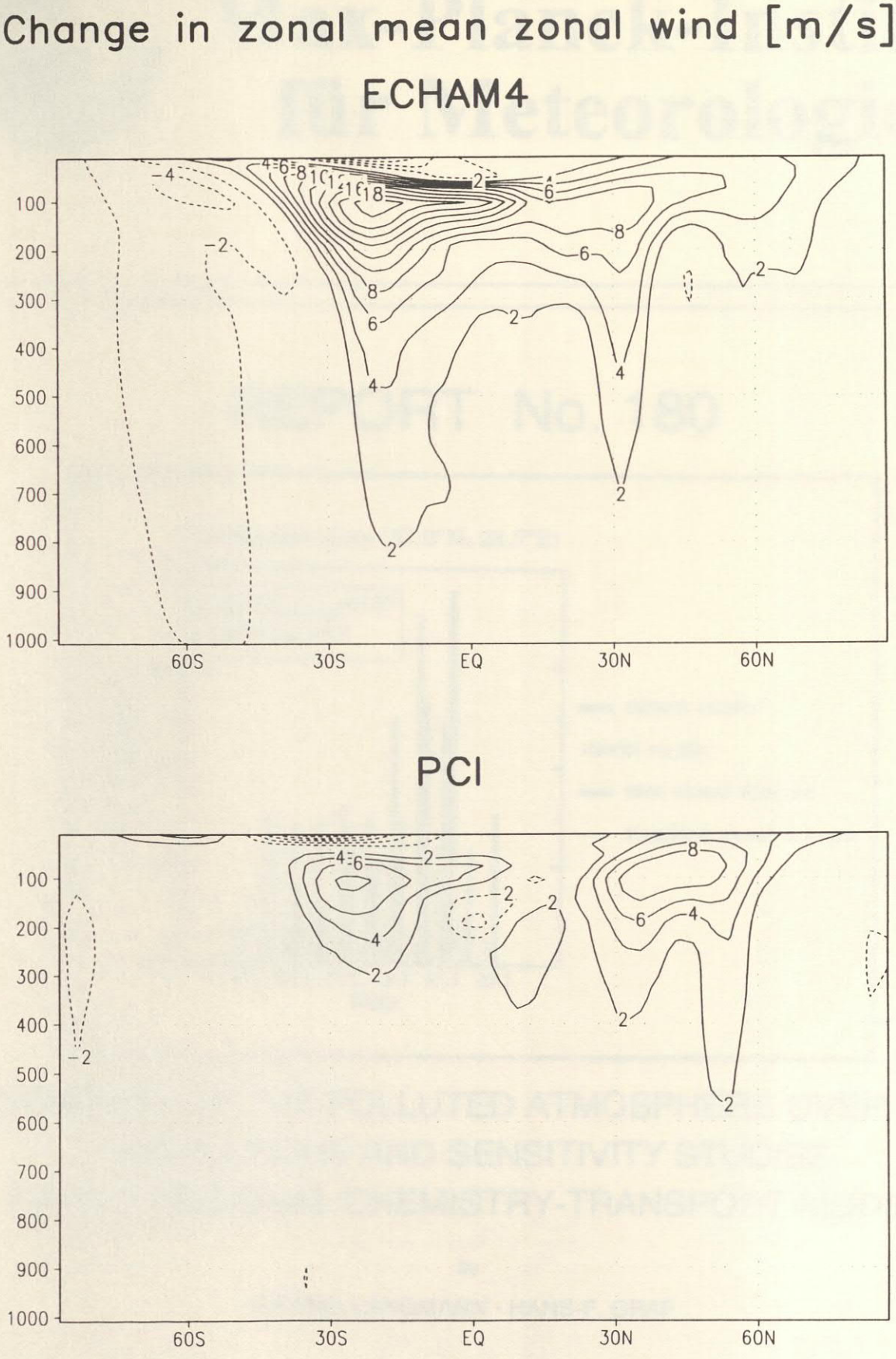

Figure 12: Latitude-pressure cross section of the difference in zonal mean zonal wind between the SST+2K and the SST-2K experiments for ECHAM4 (upper panel) and PCI (lower panel).